# Determining the Burgers vectors and elastic strain energies of interface dislocation arrays using anisotropic elasticity theory

A.J. Vattré[a,b,*], M.J. Demkowicz[b]

[a] *CEA, DAM, DIF, F-91297 Arpajon, France*
[b] *MIT, Department of Materials Science and Engineering, Cambridge MA, 02139*

**Abstract**

A general dislocation-based formalism linking the Frank-Bilby equation and heterogeneous anisotropic elasticity theory under the fundamental condition of vanishing far-field stresses is developed. The present approach gives rise to the determination of the non-arbitrary reference state, within which the Burgers vectors of individual interface dislocations are defined. A solution strategy is also formulated to predict the correct reference state in accordance with the geometric structures of interfaces and the (unequal) partitioning of elastic fields between neighboring crystals. From this dual description of interfaces, the elastic strain energies of dislocation arrays are computed using solutions of short-range fields. Examples of several simple interfaces, namely symmetric tilt and twist grain boundaries as well as pure misfit heterophase interfaces are presented.

*Keywords:* Semi-coherent interfaces, linear elasticity theory, arrays of dislocations, interface energy

## 1. Introduction

Far from being featureless dividing surfaces between neighboring crystals, interfaces in polycrystalline solids have internal structures of their own. These structures depend on interface crystallographic character (misorientation and interface plane orientation) and affect the physical and chemical properties of interfaces, such as interface energy [16], resistivity [5], diffusivity and permeability [34], mechanical properties [35], point defect sink efficiencies [50], and mobilities [38]. To better understand and control the properties of interfaces, it is desirable to be able to predict their internal structures. This paper presents a method for predicting a specific interface structural feature: the Burgers vectors of intrinsic dislocations in semicoherent grain boundaries and heterophase interfaces. This information is then used to compute interface elastic strain energies.

One way of studying interface structure is through atomistic simulations, which explicitly account for all the atoms that make up an interface. However, this approach is not always practical or efficient: it can be very resource-intensive because it requires a separate simulation for each individual interface. Thus, it does not lend itself to rapidly scanning over many different interfaces, for example if one were searching for trends in interface structures or for tailored interfaces with a specific structure. Low-cost, analytical techniques for predicting interface structure would be preferable in such situations.

One widely used analytical approach applies to semicoherent interfaces and describes interface structures in terms of intrinsic dislocations using the closely related Frank-Bilby [4, 24, 52] and O-lattice [6, 52, 57] techniques. Both procedures require the selection of a reference state, within which the Burgers vectors of individual interface dislocations are defined. Because this choice does not affect the calculated spacing and line directions of interface dislocations (see section 2.3), it has sometimes been viewed as if it were arbitrary. In practice, one of the adjacent crystals [27, 37, 56] or a "median lattice" [22] have often been used as the reference state.

However, the choice of reference state does influence the values of far-field stresses, strains, and rotations associated with interface dislocations. These, in turn, are usually subject to constraints, namely that the far-field stresses be zero and that the far-field rotations be consistent with a prescribed misorientation. Thus, the choice of reference state is in fact not arbitrary. As discussed by Hirth and co-workers [31–33], the importance of selecting proper reference states has often been overlooked in part because the best-known applications of interface dislocation models are to interfaces of relatively high symmetry, such as symmetric tilt or twist grain boundaries, for which correct reference states are easy to guess. Furthermore, many analyses assume uniform isotropic elasticity, which leads to equal partitioning of interface dislocation elastic fields between the neighboring crystals. In general, however, interfaces need not have high symmetry and the neighboring crystals may have unlike, anisotropic elastic constants. The correct selection of reference states in such general cases is far more challenging.

The purpose of the present work is to formulate an approach for determining reference states (and therefore also Burgers vectors) that give rise to predictions of interface dislocation structure whose far-field elastic fields are consistent with specified far-field stresses and constraints on the crystallographic character of semicoherent interfaces. Our method accounts for several factors that, to the best of our knowledge, have not been addressed in other studies, namely: differences in elastic constants between crystals neighboring an interface, their elastic

*Email address: aurelien.vattre@cea.fr

anisotropy, and unequal partitioning of elastic fields between them. We use our results to compute the elastic strain energies of several simple example interfaces, namely symmetric tilt and twist grain boundaries as well as pure misfit heterophase interfaces. Applications of our method to more complex interface types are to be presented in a follow-on study.

In section 2, we define certain terms used in the present work, describe our approach to modeling interface dislocations, and state the constraints on far-field elastic fields imposed by interface crystallography. Section 3 introduces our strategy for determining the Burgers vectors of interface dislocations using anisotropic elasticity theory. Section 4 presents complete solutions for elastic fields of interface dislocations. Section 5 gives applications to several examples. Section 6 provides a summary of our main results and concluding remarks.

## 2. Problem definition

In what follows in section 2, we describe our approach to modeling interface dislocations, and state the constraints imposed by interface crystallography on the achievement of equilibrium dislocation structures.

### *2.1. Planar interfaces in linear elastic bicrystals*

In our analysis, we consider planar interfaces formed by joining two semi-infinite linear elastic crystals. We assume that the crystallography of the interface has been specified completely. For a grain boundary, this requires five parameters: three to describe the relative misorientation between neighboring crystals and two to describe the orientation of the grain boundary plane [52]. For a heterophase interface, the number of crystallographic degrees of freedom may be higher. For example, an interface between two face-centered cubic (fcc) crystals such as Al and Ni would require the lattice parameters of the two neighboring metals to be given in addition to the five parameters needed for a grain boundary. Interfaces between materials with differing crystal structures may require further parameters.

To describe completely the crystallography of a heterophase interface between elements A and B, we adopt the notion of a "reference" state for the interface. In the reference state, the interface is coherent, i.e. the two separate crystals that meet at the interface are rotated and strained [36, 52] such that they are in perfect registry with each other across the interface plane after bonding, as illustrated in Fig. (1). Thus, the reference state has the interface structure of a single perfect crystal.

Starting from the reference state, materials A and B are mapped separately into new configurations that yield an interface with the required crystallographic character and zero far-field stresses, as shown in Fig. (1). Following Hirth, Pond, and co-workers [33], we refer to the state of the interface after this mapping as the "natural" state. For a grain boundary, the maps applied to materials A and B are proper rotations while for a pure misfit interface they are pure strains. To account for both cases as well as for heterophase interfaces between misoriented crystals, we describe the maps as uniform displacement gradients ${}_{\mathrm{A}}\mathbf{F}$ and ${}_{\mathrm{B}}\mathbf{F}$. In the reference state, the neighboring crystals might not be stress free, but the interface is coherent. In the natural state, the interface is not coherent, but the neighboring crystals are both free of far-field stresses.

This framework is sufficiently general to describe the crystallography of many commonly studied heterophase interfaces, e.g. ones formed by fcc and body-centered cubic (bcc) metals [16, 17], but not all. For example, mapping from a common reference state to an interface between a cubic and hexagonal close-packed crystal cannot be accomplished by a displacement gradient alone and requires an internal shuffle rearrangement as well [12]. In the present work, we restrict ourselves to materials that may be mapped to a common reference state using displacement gradients alone.

The crystallographic considerations described above do not require a single, unique reference state. On the contrary, an infinite number of new reference states may be generated from an original one by applying to it any uniform displacement gradient ${}_{\mathrm{R}}\mathbf{F}$. If the original reference state may be mapped to the natural state with ${}_{\mathrm{A}}\mathbf{F}$ and ${}_{\mathrm{B}}\mathbf{F}$, then the new reference state may be mapped to the same natural state using ${}_{\mathrm{A}}\mathbf{F}\,{}_{\mathrm{R}}\mathbf{F}^{-1}$ and ${}_{\mathrm{B}}\mathbf{F}\,{}_{\mathrm{R}}\mathbf{F}^{-1}$. However, a consistent description of the elastic fields of a discrete dislocation network in an interface of specified crystallography and free of far-field stresses does require a single specific reference state.

### *2.2. Volterra dislocations in the reference state*

The atomic structures of real interfaces are not like those generated by the linear mappings from a reference state. Instead, for any given interface crystallography, the atomic structure may undergo a variety of local relaxations or reconstructions that lower its energy. In many low-misorientation grain boundaries and low-misfit heterophase interfaces, these changes lead to formation of regions of coherency (which generally have low energies) separated by networks of dislocations. Many such interface dislocation networks have been imaged using transmission electron microscopy [1].

There are two common ways of describing interface dislocations. In one, they are viewed not as conventional Volterra dislocations, but rather as special kinds of interface defects with short-range elastic fields that are formed when the interface atomic structure in the natural state relaxes [8, 28]. The superimposed elastic fields of all such defects residing within an interface decay away to zero at long range and therefore do not alter the far-field stress state or the crystallography of the natural interface state.

Another description—the one we adopt here—views interface dislocations as genuine Volterra dislocations with resultant elastic stress and strain fields that need not decay to zero at long range. For example, the structure of some pure misfit heterophase interfaces may be described as an array of equally spaced edge dislocations residing on the same glide plane [42]. It may be shown that such an array of Volterra dislocations has a non-zero far-field stress [30]. Certain symmetric tilt grain boundaries may be described as arrays of edge dislocations lying directly one above the other on separate glide planes. Such Volterra dislocation arrays have zero far-field strains (hence, also zero stresses), but non-zero far-field rotations [39, 48]. In

general, arrays of Volterra dislocations may have non-zero far-field strains, rotations, or both.

In the work described here, we model interface dislocations as Volterra dislocations that have been introduced into the reference state, as shown in Fig. (1). We require that the far-field stresses due to these dislocations ${}_{\text{A}}\boldsymbol{\sigma}^{\infty}_{\text{dis}}$ and ${}_{\text{B}}\boldsymbol{\sigma}^{\infty}_{\text{dis}}$ are equal and opposite to the coherency stresses ${}_{\text{A}}\boldsymbol{\sigma}_{\text{c}}$ and ${}_{\text{B}}\boldsymbol{\sigma}_{\text{c}}$ in the reference state respectively, leading to the removal of all far-field stresses in the natural state:

$$ {}_{\text{A}}\boldsymbol{\sigma}_{\text{c}} + {}_{\text{A}}\boldsymbol{\sigma}^{\infty}_{\text{dis}} = \mathbf{0} \quad \text{and,} \quad {}_{\text{B}}\boldsymbol{\sigma}_{\text{c}} + {}_{\text{B}}\boldsymbol{\sigma}^{\infty}_{\text{dis}} = \mathbf{0} \, . \tag{1} $$

Although free of long-range stresses, interface dislocation networks in the natural state have non-zero short-range elastic fields as a result of the superposition of the non-uniform stress fields of the Volterra dislocation networks and the uniform coherency stresses in the reference state. Additionally, the far-field rotations due to the Volterra dislocations are required to conform to the given interface crystallographic character. These requirements restrict the choice of reference states to a single specific one.

We treat the notion of introducing Volterra dislocations into the reference state primarily as a hypothetical operation. However, this operation may be a physically meaningful analog of processes occurring at some real interfaces. For example, the transformation of certain coherent heterophase interfaces into ones that are not coherent, but free of far-field stresses, occurs by the deposition on the interface of Volterra dislocations that glide through the neighboring crystalline layers [42–45]. Similarly, subgrain boundaries are thought to assemble from glide dislocations formed during plastic deformation of polycrystals [2].

### *2.3. Crystallographic constraints on interface dislocations*

A variety of shapes of interface dislocation networks have been observed [1], but here we will limit ourselves to ones that may be represented by $j \leq 2$ arrays of parallel dislocations with Burgers vectors $\boldsymbol{b}_i$, line directions $\boldsymbol{\xi}_i$, and inter-dislocation spacings $d_i$. Following previous investigators [4, 24, 52], we relate these quantities to the density of admissible Volterra dislocations in the reference state and interface crystallography as

$$ \boldsymbol{B} = \sum_{i=1}^{j} \left( \frac{\boldsymbol{n} \times \boldsymbol{\xi}_i}{d_i} \cdot \boldsymbol{p} \right) \boldsymbol{b}_i = \left( {}_{\text{A}}\mathbf{F}^{-1} - {}_{\text{B}}\mathbf{F}^{-1} \right) \boldsymbol{p} = \mathbf{T}\boldsymbol{p} \, , \tag{2} $$

where $\boldsymbol{n}$ is a unit vector normal to the interface and the so-called probe vector $\boldsymbol{p}$ is any vector contained within the interface plane. Eq. (2) is known as the quantized Frank-Bilby equation [52, 56], where $\mathbf{T}$ corresponds to an average operation that maps $\boldsymbol{p}$ to $\boldsymbol{B}$: the resultant Burgers vector of interface dislocations intersected by $\boldsymbol{p}$.

The individual Burgers vectors $\boldsymbol{b}_i$ of interface dislocations are assumed to be related to the crystal structure of the reference state. For example, if the reference state is an fcc crystal of lattice parameter $a$, values of $\boldsymbol{b}_i$ may be drawn from a set of $\frac{a}{2}\langle 110 \rangle$-type glide or $\frac{a}{6}\langle 112 \rangle$-type Shockley partial dislocation Burgers vectors. Once the set of admissible Burgers vectors is known, well-studied methods stemming from Bollmann's O-lattice theory [6] may be used to compute $\boldsymbol{n}$, $\boldsymbol{\xi}_i$, and $d_i$ [37, 56] from the O-lattice vectors $\boldsymbol{p}^{\text{o}}_i$, defined by

$$ \boldsymbol{b}_i = \mathbf{T}\boldsymbol{p}^{\text{o}}_i \, . \tag{3} $$

The O-lattice vectors $\boldsymbol{p}^{\text{o}}_i$—and therefore both $\boldsymbol{\xi}_i$ and $d_i$—do not depend on the choice of reference state. If an original reference state is mapped to a new one using displacement gradient ${}_{\text{R}}\mathbf{F}$, then $\boldsymbol{b}_i$ is mapped to $\check{\boldsymbol{b}}_i = {}_{\text{R}}\mathbf{F}\boldsymbol{b}_i$. Here and in the following, the superimposed inverse caret will be used to indicate arbitrary quantities. The new reference state may also be mapped to the natural state using ${}_{\text{A}}\check{\mathbf{F}} = {}_{\text{A}}\mathbf{F}\,{}_{\text{R}}\mathbf{F}^{-1}$ and ${}_{\text{B}}\check{\mathbf{F}} = {}_{\text{B}}\mathbf{F}\,{}_{\text{R}}\mathbf{F}^{-1}$, as discussed in section 2.1. Assuming that rank $\mathbf{T} = 3$, the O-lattice vectors computed from the original and new reference states are identical:

$$ \boldsymbol{p}^{\text{o}}_i = \mathbf{T}^{-1}\boldsymbol{b}_i = \left( {}_{\text{A}}\check{\mathbf{F}}^{-1} - {}_{\text{B}}\check{\mathbf{F}}^{-1} \right)^{-1} \check{\boldsymbol{b}}_i = \check{\boldsymbol{p}}^{\text{o}}_i \, . \tag{4} $$

This conclusion may also be shown for matrix $\mathbf{T}$ of rank 2. Thus, for a given set of Burgers vectors $\boldsymbol{b}_i$, interface crystallography uniquely determines interface dislocation line directions $\boldsymbol{\xi}_i$ and spacings $d_i$, but not the reference state. Based on this result, some authors have argued that the choice of reference state is truly arbitrary [6]. However, in different reference states, $\boldsymbol{b}_i$ will clearly have different magnitudes and directions, both of which influence the magnitudes of the elastic fields generated by interface dislocations (the latter by altering their characters).

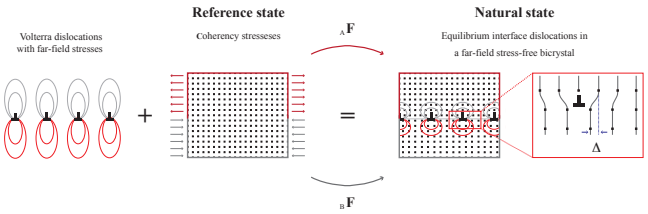


Figure 1: Mapping from a coherent reference state to the natural state using displacement gradients ${}_{\text{A}}\mathbf{F}$ and ${}_{\text{B}}\mathbf{F}$. Volterra dislocations introduced into the reference state remove coherency stresses and may change the relative rotation of the neighboring crystals.

## 3. Solution strategy

Determining the elastic energy of semicoherent interfaces requires finding the correct interface dislocation Burgers vectors, which are defined in the coherent reference state, as described in section 2. To determine the specific reference state that meets the constraints of interface crystallographic character and zero far-field stresses, we will follow the five-step strategy given below.

*Step 1: Solving for geometry of dislocation networks*

As shown in section 2.3, the geometry of interface dislocations (their spacings and line directions) is independent of the choice of reference state. Thus, we choose a reference

state identical to one of the crystals adjacent to the interface in its natural state. This choice provides an initial guess of the interface dislocation Burgers vectors. We then proceed to determine interface dislocation geometry using standard methods [7, 27, 37]. Multiple dislocation geometries are possible in some interfaces, but here we restrict attention to interfaces with unique geometries.

*Step 2: Solving for interface dislocation elastic fields*

The complete elastic fields, produced by the arrays of dislocations found in *step 1*, are determined using anisotropic linear elasticity theory in bicrystals. The periodicity of the elastic fields is assumed to follow that of the two-dimensional dislocation structures predicted in *step 1* that must also satisfy specific boundary conditions at the interfaces.

*Step 3: Solving for far-field distortions*

The far-field distortions associated with each set of parallel dislocations are computed separately and then superimposed to obtain the resultant far-field distortions. These elastic distortions are key for determining the correct reference state for the interfaces of interest in anisotropic bicrystals. Far-field strains, stresses, and rotations may also be deduced.

*Step 4: Solving for the reference state*

The correct reference state is the one in which the superposition of the strains produced by interface dislocation arrays eliminate the coherency strains, giving a bicrystal that is free of far-field stresses and has far-field rotations that agree with the given interface crystallographic character. This condition is met by continuously adjusting the reference state, starting with the initial guess selected in *step 1*.

*Step 5: Solving for the interface elastic strain energy*

Incomplete cancellation of the coherency and Volterra fields near the interface give rise to short-range stresses and strains. These stresses and strains are used to compute the elastic energies of semicoherent interfaces.

## 4. Elastic fields of interface dislocation arrays

The model is used to quantify an interface created by bonding two materials A and B, and containing up to two arrays of straight parallel dislocations at equilibrium, as illustrated in Fig. (2a). We use the Stroh formalism of anisotropic linear elasticity [13, 18, 51] and a Fourier series-based solution technique to compute the elastic fields outside the cores of interface dislocations [3, 9, 10, 15]. For clarity, the pre-subscripts A and B in the field expressions will be omitted in this section if no distinction between materials is required.

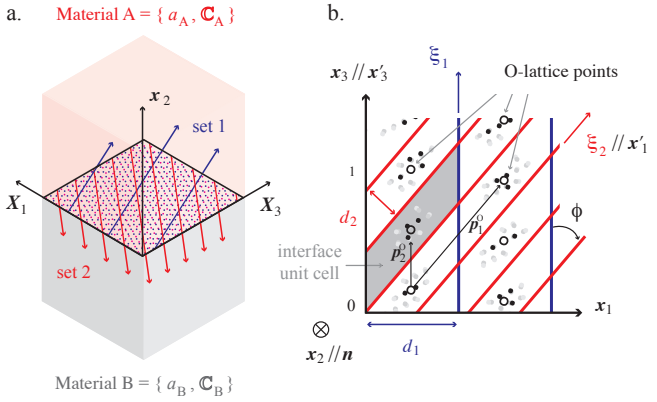


Figure 2: (a) Schematic illustration of a planar interface dislocation network formed by bonding materials A and B. (b) The geometry of an interface containing two sets of dislocations described by O-lattice vectors $\boldsymbol{p}_1^{\mathrm{o}}$ and $\boldsymbol{p}_2^{\mathrm{o}}$. Open circles represent O-lattice points and filled circles illustrate atoms with nearly matching positions in materials A and B.

### 4.1. Problem formulation

The geometry of a dislocation network consisting of two arrays of straight parallel dislocations may be described by two O-lattice vectors $\boldsymbol{p}_1^{\mathrm{o}} \neq \boldsymbol{p}_2^{\mathrm{o}}$ in the interface of interest using a Cartesian coordinate system with basis vectors $(\boldsymbol{x}_1, \boldsymbol{x}_2, \boldsymbol{x}_3)$, as shown in Fig. (2b). An interface containing only one array of straight parallel dislocations is a special case of this more general geometrical description. The unit vector normal to the interface is $\boldsymbol{n} \parallel \boldsymbol{x}_2$, with the interface located at $x_2 = 0$, $x_2 > 0$ for material A, and $x_2 < 0$ for material B. The dislocation line direction $\boldsymbol{\xi}_1$ is parallel to $\boldsymbol{p}_2^{\mathrm{o}}$ and $\boldsymbol{\xi}_2 \parallel \boldsymbol{p}_1^{\mathrm{o}}$, as illustrated in numerous references [27, 52, 56].

A representative unit cell of the dislocation pattern is illustrated in Fig. (2b). Translations of the unit cell by the basis vectors $\boldsymbol{p}_1^{\mathrm{o}}$ and $\boldsymbol{p}_2^{\mathrm{o}}$ tessellate the interface plane. It is also convenient to identify a non-orthogonal (oblique) frame with basis vectors $(\boldsymbol{x}'_1, \boldsymbol{x}_2, \boldsymbol{x}'_3)$, where $\boldsymbol{x}'_1 \parallel \boldsymbol{p}_1^{\mathrm{o}} \parallel \boldsymbol{\xi}_2$ and $\boldsymbol{x}'_3 \parallel \boldsymbol{x}_3 \parallel \boldsymbol{p}_2^{\mathrm{o}} \parallel \boldsymbol{\xi}_1$. The oriented angle between $\boldsymbol{\xi}_2$ and $\boldsymbol{\xi}_1$ is denoted by $\phi$, so that $x'_1 = x_1 \csc\phi$ and $x'_3 = x_3 - x_1 \operatorname{ctg}\phi$. Thus, any position vector in this non-orthogonal frame may be expressed as $\boldsymbol{r} = x'_1 \boldsymbol{p}_1^{\mathrm{o}} + x'_3 \boldsymbol{p}_2^{\mathrm{o}}$.

Due to the periodicity of the interface dislocation structure, it is useful to seek a complete set of wavevectors $\boldsymbol{k}$ such that the elastic fields in the interface may be analyzed using plane waves $\mathrm{e}^{i2\pi \boldsymbol{k}\cdot\boldsymbol{r}}$. The set of all $\boldsymbol{k}$ is conveniently written as $\boldsymbol{k} = n\boldsymbol{p}_1^{\times} + m\boldsymbol{p}_2^{\times}$ with respect to the reciprocal vectors $\boldsymbol{p}_1^{\times}$ and $\boldsymbol{p}_2^{\times}$, defined by the orthogonality conditions $\boldsymbol{p}_\alpha^{\times} \cdot \boldsymbol{p}_\beta^{\mathrm{o}} = \delta_{\alpha\beta}$, where $\delta_{\alpha\beta}$ is the Kronecker delta and $n$, $m$ are integers.

The complete elastic distortion field $\mathbf{D}_{\mathrm{tot}}$ is the superposition of the uniform coherency and the Volterra dislocation distortions, $\mathbf{D}_{\mathrm{c}}$ and $\mathbf{D}_{\mathrm{dis}}$, as discussed in section 2.2. Following Bonnet [9, 10], outside of dislocation cores, $\mathbf{D}_{\mathrm{tot}}$ may be expressed as the biperiodic Fourier series

$$\mathbf{D}_{\mathrm{tot}}(\boldsymbol{x}) = \mathbf{D}_{\mathrm{c}} + \mathbf{D}_{\mathrm{dis}}(\boldsymbol{x}) = \mathbf{D}_{\mathrm{c}} + \sum_{\boldsymbol{k}\neq\boldsymbol{0}} \mathrm{e}^{i2\pi\boldsymbol{k}\cdot\boldsymbol{r}}\, \mathbf{D}_{\boldsymbol{k}}(x_2)\ , \tag{5}$$

where $i = \sqrt{-1}$ and the sum spans over all non-zero wavevectors $\boldsymbol{k}$. The Fourier amplitudes of the complete distortion waves

$\mathbf{D}_{\boldsymbol{k}}(x_2)$ are required to converge (not necessary to zero) in the far-field, i.e. $x_2 \to \pm\infty$. The components $k_1$ and $k_3$ of the wavevector $\boldsymbol{k}$ satisfy

$$\boldsymbol{k}\cdot\boldsymbol{r} = k_1\, x_1 + k_3\, x_3 = \left(\frac{n\,\csc\phi}{|\boldsymbol{p}_1^{\circ}|} - \frac{m\,\mathrm{ctg}\,\phi}{|\boldsymbol{p}_2^{\circ}|}\right) x_1 + \frac{m}{|\boldsymbol{p}_2^{\circ}|}\, x_3\ . \quad (6)$$

The complete displacement field $\boldsymbol{u}_{\text{tot}}$ may be found by integrating eq. (5):

$$\begin{aligned}\boldsymbol{u}_{\text{tot}}(\boldsymbol{x}) &= \underbrace{\boldsymbol{u}_0 + \mathbf{D}_{\text{c}}\,\boldsymbol{x}}_{\text{affine part}} + \sum_{\boldsymbol{k}\neq\boldsymbol{0}} \mathrm{e}^{i2\pi\boldsymbol{k}\cdot\boldsymbol{r}}\,\boldsymbol{u}_{\boldsymbol{k}}(x_2) \\ &= \boldsymbol{u}_{\text{aff}}(\boldsymbol{x}) + \boldsymbol{u}_{\text{dis}}(\boldsymbol{x})\ ,\end{aligned} \quad (7)$$

where $\boldsymbol{u}_0$ is an arbitrary constant displacement. The field $\boldsymbol{u}_{\text{tot}}$ may be decomposed into an affine part $\boldsymbol{u}_{\text{aff}}$ corresponding to $\mathbf{D}_{\text{c}}$ and a biperiodic Fourier series representation of displacement fields $\boldsymbol{u}_{\text{dis}}$ generated by the Volterra dislocations.

The Fourier amplitudes in eqs. (5) and (7) are determined from linear elasticity in the absence of body forces and subject to boundary conditions associated with interface dislocations. The complete displacement gradients $\mathbf{D}_{\text{tot}}(\boldsymbol{x}) = \text{grad}\,\boldsymbol{u}_{\text{tot}}(\boldsymbol{x})$ in crystals A and B must fulfill the partial differential equations of mechanical equilibrium

$$\text{div}\,(\mathbb{C} : \text{grad}\,\boldsymbol{u}_{\text{tot}}(\boldsymbol{x})) = \boldsymbol{0}\ , \quad (8)$$

where : denotes the double inner product and $\mathbb{C}$ is a fourth-order anisotropic elasticity tensor.

### *4.2. Complete field solutions*

Substituting the displacement field eq. (7) into eq. (8), the second-order differential equation applied to both half-spaces is obtained as follows

$$w_1\mathbf{W}_1\,\boldsymbol{u}_{\boldsymbol{k}}(x_2) + w_2\left(\mathbf{W}_2 + \mathbf{W}_2^{\text{t}}\right)\frac{\partial\boldsymbol{u}_{\boldsymbol{k}}(x_2)}{\partial x_2} + \mathbf{W}_3\,\frac{\partial^2\boldsymbol{u}_{\boldsymbol{k}}(x_2)}{\partial x_2^2} = \boldsymbol{0}\ . \quad (9)$$

with $w_1 = -4\pi^2$ and $w_2 = i2\pi$. Here, $^{\text{t}}$ denotes the matrix transpose and $\mathbf{W}_1$, $\mathbf{W}_2$, and $\mathbf{W}_3$ are $3\times 3$ real matrices related to the wavevectors (i.e. interface geometry) and the stiffness constants (i.e. elasticity) indexed in Voigt notation:

$$\begin{aligned}\mathbf{W}_1 &= \mathbf{W}_1^{\text{t}} \\ &= \begin{bmatrix} k_1^2c_{11} + 2k_1k_3c_{15} + k_3^2c_{55} & k_1^2c_{16} + k_1k_3(c_{14}+c_{56}) + k_3^2c_{45} & k_1^2c_{15} + k_1k_3(c_{13}+c_{55}) + k_3^2c_{35} \\ & k_1^2c_{66} + 2k_1k_3c_{46} + k_3^2c_{44} & k_1^2c_{56} + k_1k_3(c_{36}+c_{45}) + k_3^2c_{34} \\ \text{sym} & & k_1^2c_{55} + 2k_1k_3c_{35} + k_3^2c_{33}\end{bmatrix}\end{aligned}$$

$$\mathbf{W}_2 = \begin{bmatrix} k_1c_{16} + k_3c_{56} & k_1c_{12} + k_3c_{25} & k_1c_{14} + k_3c_{45} \\ k_1c_{66} + k_3c_{46} & k_1c_{26} + k_3c_{24} & k_1c_{46} + k_3c_{44} \\ k_1c_{56} + k_3c_{36} & k_1c_{25} + k_3c_{23} & k_1c_{45} + k_3c_{34}\end{bmatrix}$$

$$\mathbf{W}_3 = \mathbf{W}_3^{\text{t}} = \begin{bmatrix} c_{66} & c_{26} & c_{46} \\ & c_{22} & c_{24} \\ \text{sym} & & c_{44}\end{bmatrix}\ .$$

(10)

As demonstrated in Appendix A, the complete displacement field (7) may be written as expressed in eq. (A-5), i.e.

$$\begin{aligned}\boldsymbol{u}_{\text{tot}}(\boldsymbol{x}) = \boldsymbol{u}_0 + \mathbf{D}_{\text{c}}\,\boldsymbol{x} + \frac{1}{i2\pi}\sum_{\boldsymbol{k}\neq\boldsymbol{0}} \mathrm{e}^{i2\pi\boldsymbol{k}\cdot\boldsymbol{r}} \\ \times \sum_{\alpha=1}^{3} \lambda^{\alpha}\mathrm{e}^{i2\pi p^{\alpha}x_2}\,\boldsymbol{a}^{\alpha} + \zeta^{\alpha}\mathrm{e}^{i2\pi p_*^{\alpha}x_2}\,\boldsymbol{a}_*^{\alpha}\ ,\end{aligned} \quad (11)$$

where the eigenvalues $p^{\alpha}$ and eigenvectors $\boldsymbol{a}^{\alpha}$ are calculated by solving the sextic equation (A-3) and the homogeneous linear system of equations (A-2), respectively. The asterisk indicates complex conjugates of solutions with positive imaginary parts, i.e. $p^{\alpha+3} = p_*^{\alpha}$ and $\boldsymbol{a}^{\alpha+3} = \boldsymbol{a}_*^{\alpha}$, indexed by $\alpha = 1, 2, 3$. The complete elastic strains and stresses are also deduced from eq. (11) by

$$\begin{aligned}\mathbf{E}_{\text{tot}}(\boldsymbol{x}) &= \{\mathbf{D}_{\text{tot}}(\boldsymbol{x})\} = \tfrac{1}{2}\left(\text{grad}\,\boldsymbol{u}_{\text{tot}}(\boldsymbol{x}) + \text{grad}\,\boldsymbol{u}_{\text{tot}}^{\text{t}}(\boldsymbol{x})\right) \\ \boldsymbol{\sigma}_{\text{tot}}(\boldsymbol{x}) &= \mathbb{C} : \mathbf{E}_{\text{tot}}(\boldsymbol{x})\ ,\end{aligned} \quad (12)$$

respectively. Eq. (12a) gives the strain−displacement relationship, where $\{\mathbf{D}_{\text{tot}}(\boldsymbol{x})\}$ denotes the symmetric component of the distortion field, given by eq. (A-6). Eq. (12b) is the generalized Hooke's law for small strains that determines the stress field, as expressed in eq. (A-8).

The general solutions of elastic fields of eqs. (11−12) are expressed as linear combinations of the eigenfunctions given by eq. (A-1), and include $\lambda^{\alpha}$ and $\zeta^{\alpha}$ as complex unknown quantities that are to be determined by the boundary conditions.

The two following sections describe the boundary conditions associated with equilibrium interface dislocations: *conditions 1.* and *2.* deal with the far-field elastic fields (section 4.3) while *conditions 3.* and *4.* are focused on specific requirements at the interface (section 4.4).

### *4.3. Far-field boundary conditions*

*Condition 1: Convergence of elastic fields*

In accordance with Saint Venant's principle, the convergence of the Fourier amplitudes $\boldsymbol{u}_{\boldsymbol{k}}(x_2)$ when $x_2 \to \pm\infty$ leads to the requirement that ${}_{\text{A}}\zeta^{\alpha} = 0$ and ${}_{\text{B}}\lambda^{\alpha} = 0$. This condition applies to infinite bicrystals and would not be appropriate for bicrystals terminated with free-surfaces.

*Condition 2: Absence of strains in the far-fields*

The elimination of the coherency strains $\mathbf{E}_{\text{c}}$ by the far-field strains of the interface Volterra dislocations $\mathbf{E}_{\text{dis}}^{\infty}$ is taken into account by decaying to zero the total elastic strain field $\mathbf{E}_{\text{tot}}$ when $x_2 \to \pm\infty$, i.e.

$$\lim_{x_2\to\pm\infty} \mathbf{E}_{\text{tot}}(\boldsymbol{x}) = \mathbf{E}_{\text{tot}}^{\infty} = \mathbf{E}_{\text{c}} + \mathbf{E}_{\text{dis}}^{\infty} = \boldsymbol{0}\ , \quad (13)$$

where $\mathbf{E}_{\text{c}} = \{\mathbf{D}_{\text{c}}\}$ and $\mathbf{E}_{\text{dis}}^{\infty} = \{\mathbf{D}_{\text{dis}}^{\infty}\}$ is the far-field strain produced by the interface dislocations. Eq. (13) is equivalent to eqs. (1) expressed using strains rather than stresses. As shown in Appendix B, the far-field distortions, calculated individually

for each set of dislocations, $i = 1$ and 2, and then superposed, are given by eq. (B-10) as

$$\mathbf{D}^{\infty}_{\text{dis}} = -\text{sgn}\,(x_2)\ \text{Re}\sum_{i=1}^{2} d_i^{-1}\sum_{\alpha=1}^{3}\bar{\lambda}_i^{\alpha}\mathbf{G}_i^{\alpha}+\bar{\zeta}_i^{\alpha}\mathbf{G}_{i*}^{\alpha}\ . \tag{14}$$

Here, ${}_{\text{A}}\bar{\zeta}_1^{\alpha} = {}_{\text{A}}\bar{\zeta}_2^{\alpha} = 0$ and ${}_{\text{B}}\bar{\lambda}_1^{\alpha} = {}_{\text{B}}\bar{\lambda}_2^{\alpha} = 0$ for the reasons described in boundary condition 1. Superimposed bars are used to indicate quantities related to the far-field boundary conditions, as mentioned in Appendix B. Re stands for the real part of a complex quantity. In contrast, the complex constants ${}_{\text{A}}\bar{\lambda}_i^{\alpha}$ and ${}_{\text{B}}\bar{\zeta}_i^{\alpha}$ are determined by solving the system of equations (B-17) with the aid of the complex tensors $\mathbf{G}_1^{\alpha}$ and $\mathbf{G}_2^{\alpha}$ given by eqs. (B-8) and (B-11), respectively.

*Remark 1:*

Verify Eq. (13) with the aid of eq. (14) is key for determining the correct reference state for interfaces that are free of far-field strains (or stresses) and also consistent with the Frank-Bilby and O-lattice approaches.

### *4.4. Interface boundary conditions*

*Condition 3: Disregistry due to interface Volterra dislocations*

Disregistry is the discontinuity of displacements across the interface [30] that is commonly expressed in terms of relative displacements between neighboring atomic planes. Each dislocation produces a stepwise change in disregistry whose magnitude equals its Burgers vector. The disregistry at $x_2 = 0$ of a network of two sets of dislocations may be represented by the staircase functions

$$\begin{aligned}\Delta\boldsymbol{u}_{\text{tot}}\,(x_1,x_3) &= {}_{\text{A}}\boldsymbol{u}_{\text{tot}}\,(x_1,x_3) - {}_{\text{B}}\boldsymbol{u}_{\text{tot}}\,(x_1,x_3)\\ &= -\boldsymbol{b}_1\left\lceil\frac{\csc\phi\,x_1}{|\boldsymbol{p}_1^{\text{o}}|}\right\rceil - \boldsymbol{b}_2\left\lceil\frac{x_3-\text{ctg}\,\phi\,x_1}{|\boldsymbol{p}_2^{\text{o}}|}\right\rceil\ ,\end{aligned} \tag{15}$$

as illustrated in Fig. (3), where only one set has been displayed for clarity. According to eq. (7), the complete displacement discontinuity $\Delta\boldsymbol{u}_{\text{tot}}$ at the interface is expressed as

$$\Delta\boldsymbol{u}_{\text{tot}}\,(x_1,x_3) = \Delta\boldsymbol{u}_{\text{aff}}\,(x_1,x_3) + \Delta\boldsymbol{u}_{\text{dis}}\,(x_1,x_3)\ . \tag{16}$$

The left-hand side of eq. (16) gives the relative displacement field $\Delta\boldsymbol{u}_{\text{aff}}$ at the interface generated by the uniform macroscopic distortions ${}_{\text{A}}\mathbf{D}_{\text{c}}$ and ${}_{\text{B}}\mathbf{D}_{\text{c}}$ in the affine form

$$\Delta\boldsymbol{u}_{\text{aff}}\,(x_1,x_3) = \Delta\boldsymbol{u}_0 + [\![\,({}_{\text{A}}\mathbf{D}_{\text{c}} - {}_{\text{B}}\mathbf{D}_{\text{c}})\boldsymbol{x}\,]\!]_{x_2=0}\ , \tag{17}$$

where $\Delta\boldsymbol{u}_0 = -\frac{1}{2}\,(\boldsymbol{b}_1+\boldsymbol{b}_2)$ is chosen, without loss of generality. As shown in Fig. (3), eq. (17) may be interpreted as a continuous distribution of (fictitious) Volterra dislocations with infinitesimal Burgers vectors and spacing [4, 47].

The right-hand side of eq. (16) is the displacement discontinuity $\Delta\boldsymbol{u}_{\text{dis}}$ produced by equilibrium interface dislocations in the natural state, shown as $\Delta$ in Fig. (1). According to eq. (7) and (11), the quantity $\Delta\boldsymbol{u}_{\text{dis}}$ is given by

$$\Delta\boldsymbol{u}_{\text{dis}}\,(x_1,x_3) = \frac{1}{i2\pi}\sum_{\boldsymbol{k}\neq\boldsymbol{0}}\text{e}^{i2\pi\boldsymbol{k}\cdot\boldsymbol{r}}\sum_{\alpha=1}^{3}{}_{\text{A}}\lambda^{\alpha}{}_{\text{A}}\boldsymbol{a}^{\alpha} - {}_{\text{B}}\zeta^{\alpha}{}_{\text{B}}\boldsymbol{a}_*^{\alpha}\ , \tag{18}$$

which may be represented by sawtooth functions [9, 19, 20], as illustrated in Fig. (3). Using the Fourier sine series analysis and superposing the sawtooth-shaped functions associated with the two sets of dislocations, eq. (18) can be expressed as

$$\begin{aligned}\Delta\boldsymbol{u}_{\text{dis}}\,(x_1,x_3) = &\overbrace{\sum_{n=1}^{\infty} -\frac{\boldsymbol{b}_1}{n\pi}\sin 2\pi n\frac{\csc\phi\,x_1}{|\boldsymbol{p}_1^{\text{o}}|}}^{\text{set 1}}\\ &+\underbrace{\sum_{m=1}^{\infty} -\frac{\boldsymbol{b}_2}{m\pi}\sin 2\pi m\frac{x_3-\text{ctg}\,\phi\,x_1}{|\boldsymbol{p}_2^{\text{o}}|}}_{\text{set 2}}\ .\end{aligned} \tag{19}$$

Thus, the boundary condition (19) for equilibrium interface dislocations, combined with eq. (18), leads a set of 6 linear equations

$$\Sigma_1:\ \begin{cases}\text{Re}\sum_{\alpha=1}^{3}{}_{\text{A}}\lambda^{\alpha}{}_{\text{A}}\boldsymbol{a}^{\alpha} - {}_{\text{B}}\zeta^{\alpha}{}_{\text{B}}\boldsymbol{a}_*^{\alpha} = \boldsymbol{\vartheta}\\ \text{Im}\sum_{\alpha=1}^{3}{}_{\text{A}}\lambda^{\alpha}{}_{\text{A}}\boldsymbol{a}^{\alpha} - {}_{\text{B}}\zeta^{\alpha}{}_{\text{B}}\boldsymbol{a}_*^{\alpha} = \boldsymbol{0}\ ,\end{cases} \tag{20}$$

where Im stands for the imaginary part of a complex quantity and $\boldsymbol{\vartheta}$ is given by

$$\boldsymbol{\vartheta} = \begin{cases}-\dfrac{\boldsymbol{b}_1}{n} & \text{if } m=0 \qquad (n\geq 1)\\ -\dfrac{\boldsymbol{b}_2}{m} & \text{if } n=0 \qquad (m\geq 1)\\ \boldsymbol{0} & \text{if } nm\neq 0 \qquad (n,m\geq 1)\ .\end{cases} \tag{21}$$

*Condition 4: No net tractions along the interface*

The solution must therefore satisfy the boundary condition

$${}_{\text{A}}\boldsymbol{\sigma}^{\sharp}\,(x_1,0,x_3)\,\boldsymbol{n} = {}_{\text{B}}\boldsymbol{\sigma}^{\sharp}\,(x_1,0,x_3)\,\boldsymbol{n}\ , \tag{22}$$

where $\boldsymbol{\sigma}^{\sharp}$ is the short-range stress field produced by the interface equilibrium dislocations. Following eq. (A-8), the tractions at the interface may be written as

$$\boldsymbol{\sigma}^{\sharp}\,(x_1,0,x_3)\,\boldsymbol{n} = \text{sgn}\,(x_2)\sum_{\boldsymbol{k}\neq\boldsymbol{0}}\text{e}^{i2\pi\boldsymbol{k}\cdot\boldsymbol{r}}\sum_{\alpha=1}^{3}\lambda^{\alpha}\boldsymbol{h}^{\alpha}+\zeta^{\alpha}\boldsymbol{h}_*^{\alpha}\ , \tag{23}$$

where the subsidiary complex vectors $\boldsymbol{h}^{\alpha}$ are related to the vectors $\boldsymbol{a}^{\alpha}$ by

$$\boldsymbol{h}^{\alpha} = \left(\mathbf{W}_2^{\text{t}} + p^{\alpha}\,\mathbf{W}_3\right)\boldsymbol{a}^{\alpha} = -{p^{\alpha}}^{-1}\,(\mathbf{W}_1 + p^{\alpha}\,\mathbf{W}_2)\,\boldsymbol{a}^{\alpha}\ , \tag{24}$$

with $h_k^{\alpha} = H_{k2}^{\alpha}$, as in eq. (A-10). Boundary condition (22) together with eq. (23) leads the additional system of 6 linear equations

$$\Sigma_2:\ \begin{cases}\text{Re}\sum_{\alpha=1}^{3}{}_{\text{A}}\lambda^{\alpha}{}_{\text{A}}\boldsymbol{h}^{\alpha} - {}_{\text{B}}\zeta^{\alpha}{}_{\text{B}}\boldsymbol{h}_*^{\alpha} = \boldsymbol{0}\\ \text{Im}\sum_{\alpha=1}^{3}{}_{\text{A}}\lambda^{\alpha}{}_{\text{A}}\boldsymbol{h}^{\alpha} - {}_{\text{B}}\zeta^{\alpha}{}_{\text{B}}\boldsymbol{h}_*^{\alpha} = \boldsymbol{0}\ .\end{cases} \tag{25}$$

*Remark 2:*

The elastic fields of equilibrium interface dislocations in an anisotropic bicrystal free of far-field strains are given in terms of the 12 eigenvalues Eval and 12 corresponding eigenvectors Evec with $\alpha = 1, 2, 3$, i.e.

$$\begin{aligned} \text{Eval} &= \{ \text{Re}_{\text{A}} p^\alpha, \text{Im}_{\text{A}} p^\alpha, \text{Re}_{\text{B}} p^\alpha, \text{Im}_{\text{B}} p^\alpha \} \\ \text{Evec} &= \{ {}_{\text{A}}\boldsymbol{a}^\alpha, {}_{\text{B}}\boldsymbol{a}^\alpha, {}_{\text{A}}\boldsymbol{h}^\alpha, {}_{\text{B}}\boldsymbol{h}^\alpha \} \ . \end{aligned} \tag{26}$$

All these quantities are determined by solving a 6-dimensional eigenvalue problem that may be recast with the aid of eqs. (24) into the form

$$\mathbb{N} \begin{bmatrix} \boldsymbol{a}^\alpha \\ \boldsymbol{h}^\alpha \end{bmatrix} = p^\alpha \begin{bmatrix} \boldsymbol{a}^\alpha \\ \boldsymbol{h}^\alpha \end{bmatrix} \tag{27}$$

where the real nonsymmetric $6 \times 6$ matrices $\mathbb{N}$ depend on the wavevectors and the stiffness constants for crystals A and B through the $\mathbf{W}$ matrices given by eqs. (10), i.e.

$$\mathbb{N} = \begin{bmatrix} -\mathbf{W}_3^{-1}\,\mathbf{W}_2^{\text{t}} & \mathbf{W}_3^{-1} \\ -\mathbf{W}_1 + \mathbf{W}_2\,\mathbf{W}_3^{-1}\,\mathbf{W}_2^{\text{t}} & -\mathbf{W}_2\,\mathbf{W}_3^{-1} \end{bmatrix} . \tag{28}$$

Finally, the linear systems $\Sigma_1$ and $\Sigma_2$ are solved numerically to determine the 12 real constants Ecst, i.e.

$$\text{Ecst} = \{ \text{Re}_{\text{A}} \lambda^\alpha, \text{Im}_{\text{A}} \lambda^\alpha, \text{Re}_{\text{B}} \zeta^\alpha, \text{Im}_{\text{B}} \zeta^\alpha \} \ , \tag{29}$$

completing the solutions of the elastic fields.

### *4.5. Interface elastic strain energy*

Using the divergence theorem, the elastic strain energy of equilibrium interface dislocation arrays may be expressed as a surface integral over a unit cell of the interface dislocation network [55]:

$$E_{\text{e}} = -\tfrac{1}{2} \iint_{\text{unit cell}} {}_{\text{A}}\boldsymbol{\sigma}^\sharp (x_1, 0, x_3)\, \boldsymbol{n} \cdot \Delta \boldsymbol{u}_{\text{dis}} (x_1, x_3)\ dS \ , \tag{30}$$

where ${}_{\text{A}}\boldsymbol{\sigma}^\sharp (x_1, 0, x_3)\, \boldsymbol{n}$ is the traction vector produced at the interface in material A. Stress fields at dislocation cores diverge, so regions near the cores must be excluded from the integral in eq. (30). Following standard practice [30], we limit the domain of integration to parts of the interface unit cell that are not within a pre-determined cutoff distance $r_0$ of the dislocation cores.

## 5. Example applications

Here, we apply the model described in the forgoing sections to simple example interfaces: symmetric tilt and twist grain boundaries as well as a pure misfit heterophase interface. The materials properties used in these examples are listed in Tab. (1). Interfaces with both misorientations and misfits will be treated in a separate study.

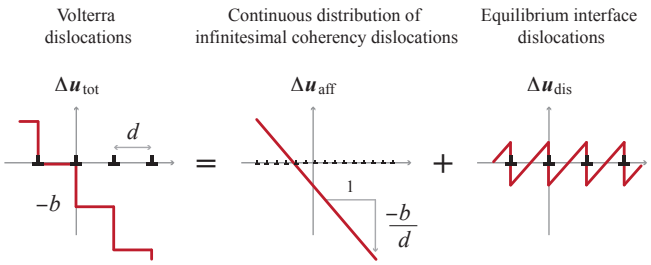


Figure 3: The disregistry $\Delta \boldsymbol{u}_{\text{tot}}$ due to interface Volterra dislocations is a staircase function. It may be decomposed into an affine part $\Delta \boldsymbol{u}_{\text{aff}}$ generated by a uniform distortion (represented by a continuous distribution of fictitious infinitesimal dislocations) and a sawtooth function $\Delta \boldsymbol{u}_{\text{dis}}$ associated with the equilibrium interface dislocations in the natural state.

| Properties | | Materials | | | | |
|---|---|---|---|---|---|---|
| Symbol | Unit | Cu | Nb | Fe | Al | Ni |
| $a$ | Å | 3.615 | 3.301 | 2.866 | 4.050 | 3.524 |
| $c_{11}$ | GPa | 168.4 | 246.0 | 242.0 | 108.2 | 246.5 |
| $c_{12}$ | GPa | 121.4 | 134.0 | 146.5 | 61.3 | 147.3 |
| $c_{44}$ | GPa | 75.4 | 28.7 | 112.0 | 28.5 | 124.7 |

Table 1: Material properties for copper, niobium, iron, aluminium, and nickel. The values of lattice parameters $a$ for all materials are those listed by Gray [26] and elastic components $c_{11}$, $c_{12}$, and $c_{44}$ by Hirth and Lothe [30].

### *5.1. Symmetric tilt grain boundary*

Pure tilt boundaries that contain one set of dislocations have been discussed extensively [52, 56]. To illustrate and validate the present method, we discuss a symmetrical tilt boundary with [001] tilt axis and tilt angle $\theta = 2°$. The calculations are carried out for Cu, which has a moderately high anisotropy ratio, $A_{\text{Cu}} = 2c_{44}/(c_{11} - c_{12}) = 3.21$. The boundary consists of one set of straight parallel dislocations with Burgers vector content $\boldsymbol{B}$ (see eq. 2) expressed as

$$\begin{aligned} \boldsymbol{B} &= \left( \frac{\boldsymbol{n} \times \boldsymbol{\xi}}{d} \cdot \boldsymbol{p} \right) \boldsymbol{b} \\ &= \underbrace{\left( \mathbf{R}_+^{-1} - \mathbf{R}_-^{-1} \right)}_{\mathbf{T}} \boldsymbol{p} = 2 \sin\theta/2\ \boldsymbol{p} \times \boldsymbol{\omega} \ . \end{aligned} \tag{31}$$

Here, we have used a "median lattice" as the obvious reference state: the mapping matrices $\mathbf{F}$ have been replaced by rotation matrices $\mathbf{R}$, with $\mathbf{R}_+$ representing a rotation of the upper crystal by angle $\theta_+ = \theta/2$ about the tilt axis and $\mathbf{R}_-$ the rotation $\theta_- = -\theta/2$ of the adjacent lower crystal. Eq. (31) is known as Frank's formula [22, 49], which gives the density of interface dislocations needed to create the tilt boundary. Selecting $\boldsymbol{b} = a_{\text{Cu}}\,[010] \parallel \boldsymbol{n}$, eq. (31) shows that $\boldsymbol{\xi} = [001]$ and $d = 10.3567$ nm.

We confirmed that the far-field stresses vanish for this choice of reference lattice, as expected, and that the only non-zero stresses are short-ranged. Fig. (4) plots interface stresses as a function of $x_1$ and $x_2$ (the stresses are invariant along the dislocation line direction, $x_3$). The red contour illustrates where the

stresses fall below $\sim 7-10$ nm (depending on the stress components), showing that their range is comparable to the dislocation spacing. The far-field rotations may be calculated from the antisymmetric part of the far-field distortions, i.e. $\mathbf{\Omega}^{\infty} = \}\mathbf{D}^{\infty}_{\rm dis}\{$. They satisfy $\mathbf{\Omega}^{\infty}_{+} - \mathbf{\Omega}^{\infty}_{-} = \mathbf{T}$ and yield a net non-vanishing rotation about the tilt axis, as excepted [29, 41]:

$$\boldsymbol{\varpi} = \boldsymbol{\varpi}^{\infty}_{+} - \boldsymbol{\varpi}^{\infty}_{-} = -\begin{pmatrix} 0 \\ 0 \\ 0.03490 \end{pmatrix} = -\frac{\boldsymbol{x}_1 \times \boldsymbol{b}}{d} \,. \tag{32}$$

The disregistry $\Delta u_{2\,\rm tot}$ and the displacement discontinuity $\Delta u_{2\,\rm dis}$ associated with the Volterra and equilibrium tilt boundary dislocations are plotted in Fig. (5a). They are in good quantitative agreement with the applied boundary conditions, represented by staircase and sawtooth curves.

The average elastic energy per unit interface area $\mathring{E}_{\rm e}$ is determined for several values of the core cutoff parameter $r_0$. Following eq. (30), $\mathring{E}_{\rm e}$ may be written as

$$\mathring{E}_{\rm e}\,(r_0) = -\frac{1}{2\,d}\int_{r_0}^{d-r_0} {}_{\rm A}\sigma^{\sharp}_{22}\,(x_1,0,0)\;\Delta u_{2\,\rm dis}\,(x_1,0)\;dx_1 \,. \tag{33}$$

The variation of stress component $\sigma^{\sharp}_{22}$ at $x_2 = 0$ with $x_1$ is plotted as a black line in Fig. (5b). The core region is shaded in grey. Local contributions to the interface elastic energy (values of the integrand in eq. 33) are plotted in red. The average elastic energy per unit interface area will depend on the choice of $r_0$. For example, $\mathring{E}_{\rm e} = 142.8$ mJ.m$^{-2}$ with $r_0 = b/2$ and $\mathring{E}_{\rm e} = 167.8$ mJ.m$^{-2}$ with $r_0 = b/3$, where $b$ is the magnitude of $\boldsymbol{b}$. We attempt to determine an appropriate $r_0$ value by comparing the interface elastic energies computed with our method to experimentally measured energies of small angle [001] tilt boundaries [25], plotted as solid triangles in Fig. (6). Our calculations using $r_0 = b/2$ are in good agreement with the experiments up to $\sim 5^{\circ}$ while $r_0 = b/3$ fits better in the range of $\sim 5-12^{\circ}$. The classical energy per unit area given by Read and Shockley [48], $E_{\rm RS}\,(\theta) = 1450\;\theta\,(-3-\ln\theta)$ mJ.m$^{-2}$, is also shown in Fig. (6). It compares well with our calculations for $r_0 = b/3$.

### *5.2. Twist grain boundary*

As shown in Fig. (7a), small-angle (010) twist grain boundaries contain two sets of dislocations, so their dislocation content $\boldsymbol{B}$ is expressed as

$$\begin{aligned} \boldsymbol{B} &= \left(\frac{\boldsymbol{n}\times\boldsymbol{\xi}_1}{d_1}\cdot\boldsymbol{p}\right)\boldsymbol{b}_1 + \left(\frac{\boldsymbol{n}\times\boldsymbol{\xi}_2}{d_2}\cdot\boldsymbol{p}\right)\boldsymbol{b}_2 \\ &= \left(\mathbf{R}^{-1}_{+} - \mathbf{R}^{-1}_{-}\right)\boldsymbol{p} \,. \end{aligned} \tag{34}$$

We consider twist boundaries of angle $\theta$ in Cu, where the rotation axis is perpendicular to the boundary, $\boldsymbol{\omega} = \boldsymbol{x}_2 = [010]$. As in the case of the tilt boundary, the obvious reference state for twist boundaries is the "median lattice" suggested by Frank [23]. In this state, the total rotation across the boundary is equally partitioned between the two grains. However, to illustrate the importance of selecting the correct reference state,

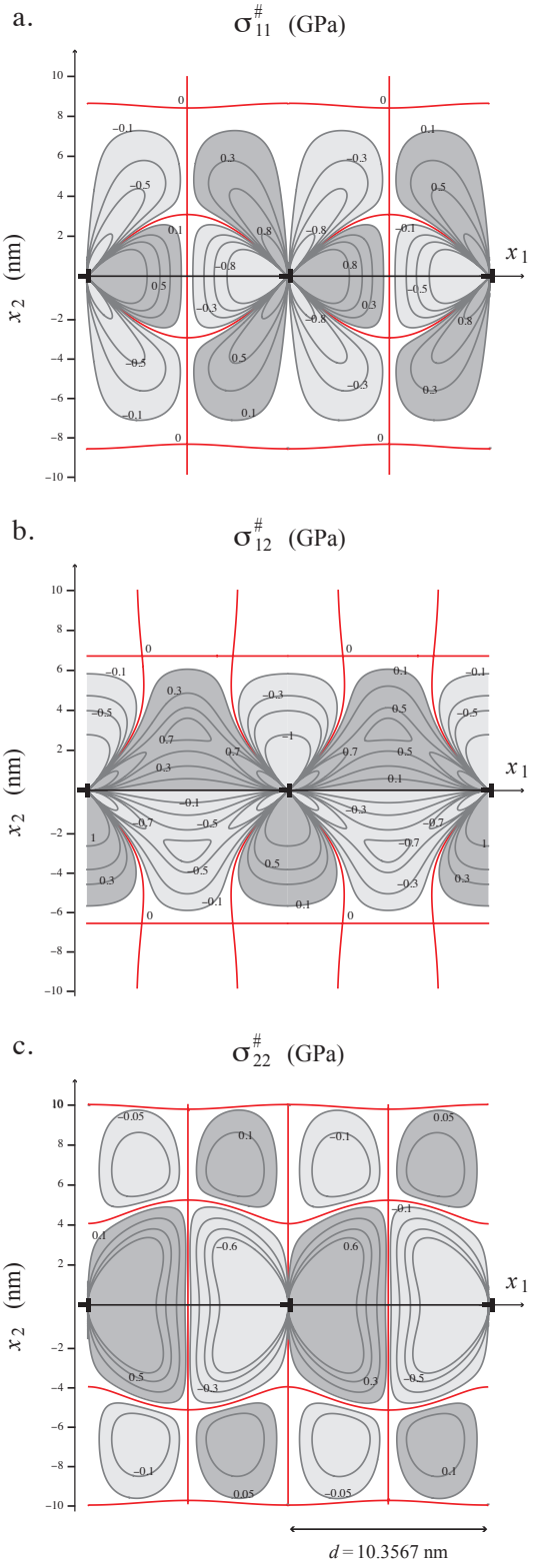


Figure 4: Contour plots of stress components (a) $\sigma^{\sharp}_{11}$, (b) $\sigma^{\sharp}_{12}$ and (c) $\sigma^{\sharp}_{22}$, for the 2° symmetric tilt boundary described in the text. The negative values (compression) are plotted in light grey, and the positive values (extension) in dark grey, via zero in red. The stresses decay away over distances comparable to the interface dislocation spacing.

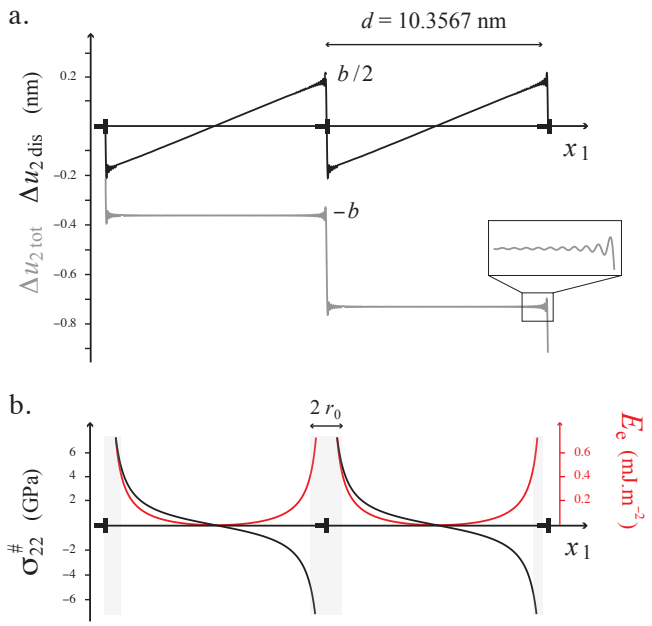


Figure 5: (a) Disregistries $\Delta u_{2\,\mathrm{tot}}$ (staircase function) and $\Delta u_{2\,\mathrm{dis}}$ (sawtooth function) computed using 100 harmonics for the 2° symmetric tilt boundary described in the text. (b) Stress distribution $\sigma^{\sharp}_{22}$ and local elastic energy density $E_{\mathrm{e}}$ at the grain boundary.

we will also consider other possible reference states. As intensely used in the literature, the two adjacent crystal lattices may be chosen as the reference lattices. There is a continuum of other possible reference states between these two extremes, so we introduce the angle $\theta_{\mathrm{c}} = -\kappa\theta$ to define the rotation of the reference state from the case where the crystal A above the boundary has been chosen as the reference lattice. Here, $\kappa$ is a dimensionless parameter that varies from 0 to 1. Equipartitioning of rotations between the adjacent crystals (i.e. the "median lattice") occurs when $\kappa = 1/2$.

Section 2.3 demonstrated that interface dislocation geometry is independent of reference state. In this example, the twist boundary contains an orthogonal grid of dislocations with line directions $\boldsymbol{\xi}_1 = 1/\sqrt{2}\,[\bar{1}01]$ and $\boldsymbol{\xi}_2 = 1/\sqrt{2}\,[101]$. The spacings between successive parallel dislocations are $d_1 = d_2 = d = 7.3233$ nm. Because of the pure twist misorientations, the coherency stress fields are zero for all possible reference states. Fig. (7) plots the dependence of non-vanishing far-field stress components on $\kappa$. If a reference state with $\kappa = 0$ is chosen, then the interface dislocations deviate by 1° from pure screw character and possess non-zero far-field stress components $\sigma^{\infty}_{11+} = \sigma^{\infty}_{33+}$ and $\sigma^{\infty}_{11-} = \sigma^{\infty}_{33-}$. This demonstrates that $\kappa = 0$ does not represent the correct reference state since eqs. (1) (and eqs. 13 via eq. 12b) are not satisfied. Furthermore, the far-field rotation with $\kappa = 0$ does not equal 2°, where an existing (small) discrepancy between the rotation vector component $\varpi_2 = -0.03489$ and the prescribed misorientation is found. As $\kappa$ increases, the far-field stresses decrease and eventually reach zero at $\kappa = 1/2$, as expected. The interface dislocations have perfect screw characters for this reference state. Non-zero far-field stresses are

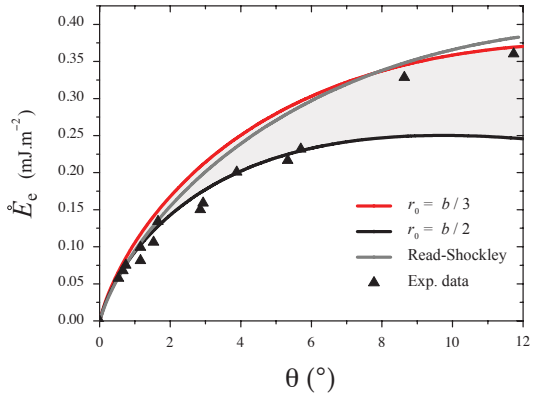


Figure 6: Interface elastic energies computed using two different core cutoff parameters $r_0$ for a [001] tilt grain boundary in Cu as a function of the tilt angle $\theta$. The gray line shows the Read-Shockley solution. Experimental values are shown with solid triangles.

again obtained when $\kappa$ is increased beyond $\kappa = 1/2$.

Taking $\kappa = 1/2$, we calculate the elastic strain energy per unit area $\mathring{E}_{\mathrm{e}}$ for the twist grain boundary using the expression:

$$\mathring{E}_{\mathrm{e}}(r_0) = -\frac{1}{2A}\iint_{r_0}^{d-r_0}\left(W_{(1)} + W_{(2)} + W_{(1-2)}\right)dx_1\,dx_3\,, \quad (35)$$

with $A = |\boldsymbol{p}^{\mathrm{o}}_1 \times \boldsymbol{p}^{\mathrm{o}}_2|$ the area of the interface unit cell. Eq. (35) is decomposed into self-energy densities $W_{(1)}$ and $W_{(2)}$ for each set of parallel dislocations and the interaction energy density $W_{(1-2)}$ between the two sets. These energies are obtained from the separate elasticity solutions for each set of dislocations:

$$\begin{aligned} W_{(1)} + W_{(2)} &= \sigma^{\sharp}_{23+(1)}(x_1,0,0)\;\Delta u_{3\,\mathrm{dis}\,(1)}(x_1,0) \\ &\quad + \sigma^{\sharp}_{12+(2)}(0,0,x_3)\;\Delta u_{1\,\mathrm{dis}\,(2)}(0,x_3) \\ W_{(1-2)} &= \sigma^{\sharp}_{23+(1)}(x_1,0,0)\;\Delta u_{1\,\mathrm{dis}\,(2)}(0,x_3) \\ &\quad + \sigma^{\sharp}_{12+(2)}(0,0,x_3)\;\Delta u_{3\,\mathrm{dis}\,(1)}(x_1,0)\;. \end{aligned} \quad (36)$$

The local self- and interaction energies are shown in Fig. (8a) and (b), respectively. The integral of the interaction energy $W_{(1-2)}$ over area $A$ is zero for any value $r_0$, in agreement with the classical dislocation theory result that orthogonal screw dislocations do not exert any forces on each other [30]. The total elastic energy is plotted in Fig. (9) as a function of the twist angle up to 12° for three core cutoff parameters: $r_0 = b_1/2$, $r_0 = b_1/3$, and $r_0 = b_1/4$.

### 5.3. *Comparison of tilt and twist grain boundary energies*

In this section, we use our model to compare the elastic energies of small-angle tilt and twist boundaries with identical [001] rotation axis. We are particularly interested in determining whether anisotropy influences which of the two has lower energy for a given misorientation. We carry out our calculations on a hypothetical iron-niobium alloy, $\mathrm{Fe}_{\chi}\mathrm{Nb}_{1-\chi}$. This is a convenient choice because Fe and Nb have similar $c_{11}$ and $c_{12}$ values, as shown in Tab. (1). Their $c_{44}$ values, however, differ markedly and therefore their anisotropy ratios do as well. We

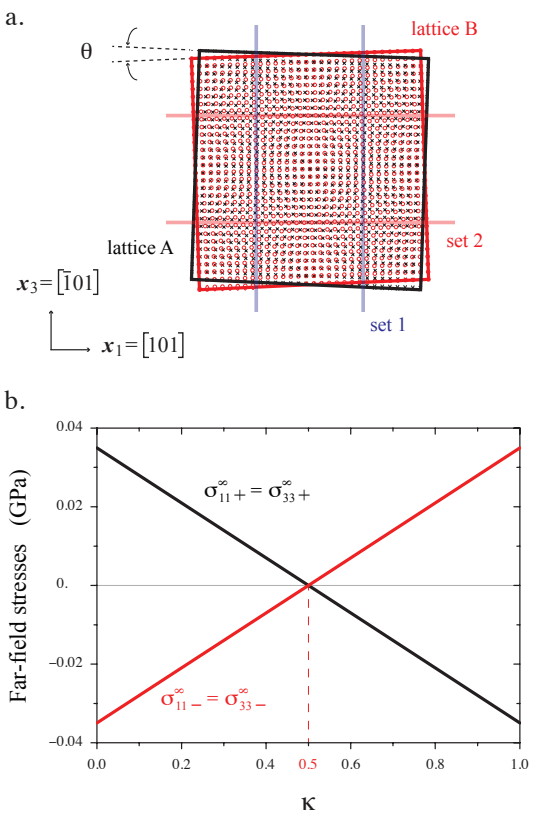


Figure 7: (a) Small-angle twist grain boundary on a (010) plane containing two sets of orthogonal dislocations. (b) Dependence of far-field stresses on $\kappa$ for the 2° twist boundary described in the text.

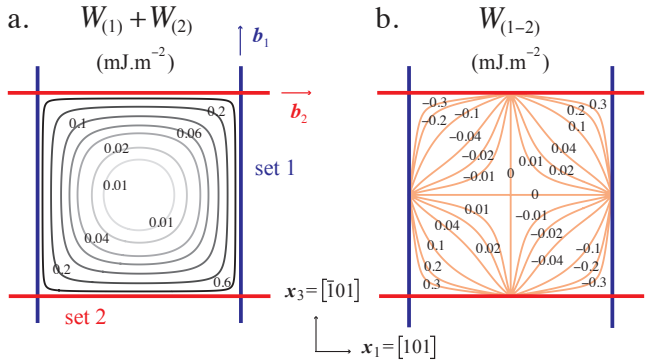


Figure 8: Local (a) self- $\{W_{(1)}+W_{(2)}\}$ and (b) interaction $W_{(1-2)}$ elastic energies arising from two sets of orthogonal screw dislocations in a 2° twist boundary on a (010) plane.

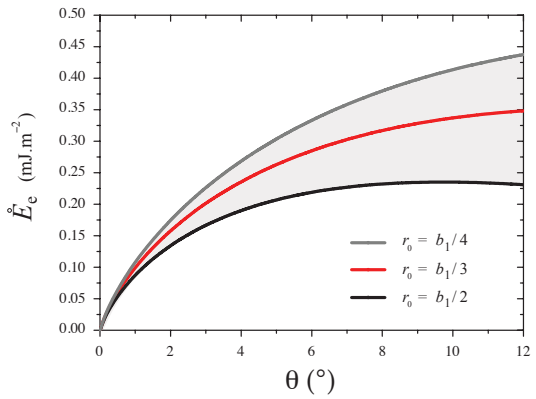


Figure 9: Elastic energies per unit area $\mathring{E}_e$ as a function of the rotation angle $\theta$ of twist grain boundaries along (010) planes in Cu for three core cutoff parameters $r_0$.

assume that the elastic constants and lattice parameters of the hypothetical $Fe_\chi Nb_{1-\chi}$ alloy are found by linear interpolation between those of Fe and Nb.

Fig. (10a) shows the elastic energies of 2° tilt and twist boundaries computed as a function of $0 \leq \chi \leq 1$ with $r_0 = b_{\text{FeNb}}/4$, $r_0 = b_{\text{FeNb}}/3$, and $r_0 = b_{\text{FeNb}}/2$. Tilt boundary energies vary roughly logarithmically with $\chi$ while twist energies increase linearly with the increasing $\chi$. Fig. (10b) illustrates a refinement of (a) over $0 \leq \chi \leq 0.2$. It is shown that the tilt boundary energy is higher than that of the twist boundary for pure Nb and for all $\chi \leq 0.09$. By contrast, the twist boundary energy is higher than the tilt boundary energy for Fe and for $\chi > 0.09$. These findings demonstrate that the relative energies of tilt and twist boundaries may be quite sensitive to anisotropy.

These calculations were performed using several different dislocation core cutoffs for edge and screw dislocations. In general, one may expect dislocations with screw character to have larger cores [30]. Inspection of Fig. (10) demonstrates that the choice of core cutoff may affect the value of $\chi$ at which the crossover in boundary energies occurs, but does not alter the qualitative conclusion that the relative energies of tilt and twist boundaries depend on anisotropy.

### 5.4. *Pure misfit interface*

Lastly, we illustrate our model on an Al−Ni heterophase interface. The terminal planes of both adjacent crystals are (010) planes. The [100] and [001] directions of both crystals are parallel in the interface plane. Thus, the interface is in the cube-on-cube orientation and contains two sets of parallel dislocations. Following eq. (2), the Burgers vector content $\boldsymbol{B}$ is written as

$$\begin{aligned}\boldsymbol{B} &= \left(\frac{\boldsymbol{n}\times\boldsymbol{\xi}_1}{d_1}\cdot\boldsymbol{p}\right)\boldsymbol{b}_1 + \left(\frac{\boldsymbol{n}\times\boldsymbol{\xi}_2}{d_2}\cdot\boldsymbol{p}\right)\boldsymbol{b}_2 \\ &= \underbrace{\left({}_{\text{Al}}\mathbf{S}^{-1}(r_{\text{Al}}) - {}_{\text{Ni}}\mathbf{S}^{-1}(r_{\text{Ni}})\right)}_{\mathbf{T}}\boldsymbol{p}\,.\end{aligned} \tag{37}$$

The reference state for this interface is a crystal oriented identically to the Al and Ni in their natural state, but strained such that its lattice constant in the interface plane is $a_c$, with $a_{\text{Ni}} \leq a_c \leq a_{\text{Al}}$. Only strains within the interface are necessary to ensure coherency: normal strains are not required. Thus, the matrix $\mathbf{T}$ in eq. (37) is composed of two equibiaxial stretch matrices (no rotations), ${}_{\text{Al}}\mathbf{S}^{-1} = {}_{\text{Al}}\mathbf{E}_c + \mathbf{I}$ and ${}_{\text{Ni}}\mathbf{S}^{-1} = {}_{\text{Ni}}\mathbf{E}_c + \mathbf{I}$, where $\mathbf{I}$ represents the identity matrix. These mapping matrices depend on

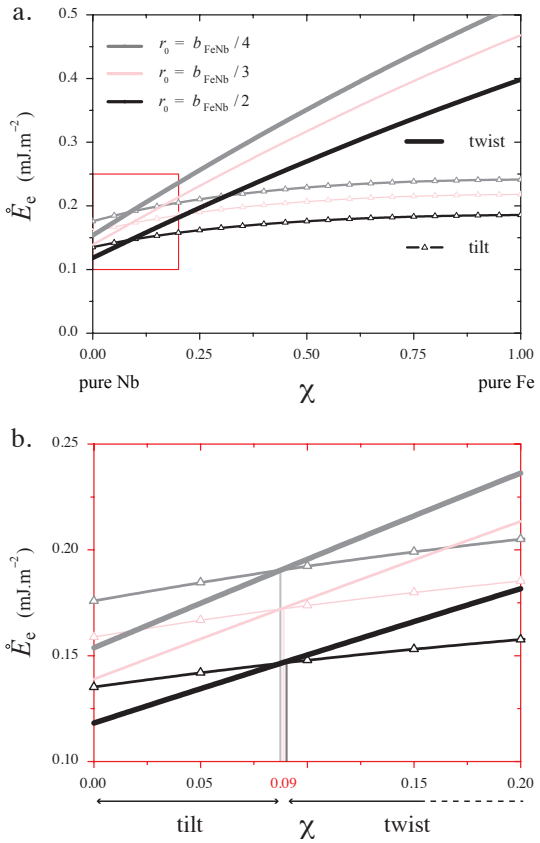


Figure 10: Elastic energies per unit area $\mathring{E}_e$ of 2° tilt and twist grain boundaries in an iron-niobium alloy, $Fe_\chi Nb_{1-\chi}$, as a function of $\chi$. Calculations are performed for three core cutoff parameters $r_0$ and plotted in the $\chi$ ranges of (a) $0 \le \chi \le 1$ and (b) $0 \le \chi \le 0.2$ for clarity.

the ratios of lattice parameters between Al and Ni in their natural and reference states, $r_{Al} = a_{Al}/a_c \ge 1$ and $r_{Ni} = a_{Ni}/a_c \le 1$.

Following the procedure described in section 3, we initially choose Ni as the reference lattice and identify $\check{\boldsymbol{b}}_1 = a_{Ni}/\sqrt{2}\,[101]$ and $\check{\boldsymbol{b}}_2 = a_{Ni}/\sqrt{2}\,[10\bar{1}]$. Then, using eq. (3), we find that $\boldsymbol{\xi}_1 = 1/\sqrt{2}\,[\bar{1}01]$ and $\boldsymbol{\xi}_2 = 1/\sqrt{2}\,[101]$, with the corresponding spacings $d_1 = d_2 = 1.902$ nm. Using this choice of reference state, we find that the far-field strains produced by the interface dislocations are:

$$
{}_{Al}\mathbf{E}^{\infty}_{dis} = \begin{bmatrix} 0.10133 & 0 & 0 \\ 0 & 0 & 0 \\ 0 & 0 & 0.10133 \end{bmatrix}
$$
$$
{}_{Ni}\mathbf{E}^{\infty}_{dis} = \begin{bmatrix} -0.03243 & 0 & 0 \\ 0 & 0 & 0 \\ 0 & 0 & -0.03243 \end{bmatrix}, \tag{38}
$$

expressed here in the principal strain axes. It is also shown that

$$
-\left({}_{Al}\mathbf{E}^{\infty}_{dis} - {}_{Ni}\mathbf{E}^{\infty}_{dis}\right) = \mathbf{T} \qquad \left(= {}_{Al}\mathbf{E}_c - {}_{Ni}\mathbf{E}_c\right) , \tag{39}
$$

which gives a necessary condition to verify eqs. (13), but not sufficient. Indeed, by combined with the prescribed coherency strains, the total far-field strains in each individual materials do not vanish, but rather equal:

$$
\begin{aligned}
{}_{Al}\mathbf{E}_c + {}_{Al}\mathbf{E}^{\infty}_{dis} &= \underbrace{{}_{Ni}\mathbf{E}_c}_{\mathbf{0}} + {}_{Ni}\mathbf{E}^{\infty}_{dis} \\
&= \begin{bmatrix} -0.03243 & 0 & 0 \\ 0 & 0 & 0 \\ 0 & 0 & -0.03243 \end{bmatrix} \neq \mathbf{0} \, .
\end{aligned} \tag{40}
$$

This demonstrates that the initial choice of reference state is not correct, since eqs. (13) are not strictly satisfied.

To find the correct reference state, we introduce a variable $\delta$, with $0 \le \delta \le 1$, that interpolates $a_c$ between $a_{Al}$ and $a_{Ni}$:

$$
a_c = \delta a_{Al} + (1-\delta)\, a_{Ni} \, . \tag{41}
$$

The $\boldsymbol{x}_1 \otimes \boldsymbol{x}_1$ total strain components $\mathbf{E}^{\infty}_{tot}$ in Al are plotted in Fig. (11) as a function of $\delta$. The $\boldsymbol{x}_3 \otimes \boldsymbol{x}_3$ components are identical to $\boldsymbol{x}_1 \otimes \boldsymbol{x}_1$ and all other strain components are zero. The same components in Ni give the same plot than in Fig. (11) −however, the individual dependence of $\mathbf{E}_c$ and $\mathbf{E}^{\infty}_{dis}$ on $\delta$ in each crystal varies differently−. The far-field strains vary linearly with $\delta$ and becomes zero when $\delta = 0.21787$, so that $a_c = 0.36386$ nm. This value of $a_c$ is closer to $a_{Ni}$ than to $a_{Al}$ because Ni is the stiffer of these two materials and so carries a lower coherency strain in the reference state. The far-field rotations are zero for all values of $\delta$.

To validate our calculation, we recompute $a_c$ under the assumption that both sides of the interface have the same stiffness (equal to that of Al or Ni), but different natural lattice parameters ($a_{Al}$ and $a_{Ni}$). The $a_c$ value we calculate for this case is in very good agreement with the well-known approximate result $\bar{a} = 2a_{Al}\,a_{Ni}\,/\,(a_{Al}+a_{Ni}) = 0.37687$ nm [24, 36, 46], corresponding to $\delta = 0.46521$. This value, however, is far from the correct lattice parameters of the reference state when the differing stiffnesses of Al and Ni are taken into account, as marked by cross symbols in Fig. (11).

To investigate the effect of the relative stiffness of the neighboring materials on the reference state, we artificially vary the value of $c_{11}$ for Al, assigning to it a value of $(\tau \times {}_{Al}c_{11})$, where ${}_{Al}c_{11}$ is $c_{11}$ for real Al and $0 \le \tau \le 30$. Fig. (12) shows that the lattice parameter of the reference state $a_c$ increases with $\tau$, i.e. as the fictitious "Al" become stiffer, and approaches the lattice parameter of real Al asymptotically. This is to be expected because, as the stiffness of a material increases, the coherency stresses it would carry in the reference state become prohibitively large, so its coherency strains must decrease. To measure the discrepancy of choosing $\bar{a}$ as the lattice parameter defined in the reference state, Fig. (12) shows that $\bar{a}$ corresponds to consider a fictitious "Al" crystal with ${}_{"Al"}c_{11}$ assigned to $\sim (8 \times {}_{Al}c_{11})$.

## 6. Concluding remarks and outlook

A general dislocation-based formalism linking the Frank-Bilby equation and anisotropic elasticity under the fundamental condition of vanishing far-field stresses and strains is developed. The present model gives rise to the determination of

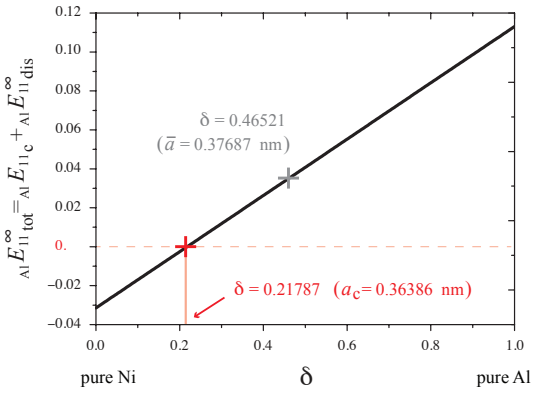


Figure 11: Dependence of the $\boldsymbol{x}_1 \otimes \boldsymbol{x}_1$ total far-field strain components $\mathbf{E}^{\infty}_{\mathrm{tot}}$ in Al on $\delta$ for a Al−Ni heterophase interface. The lattice parameter $\bar{a} = 2a_{\mathrm{Al}}\,a_{\mathrm{Ni}}\,/\,(a_{\mathrm{Al}} + a_{\mathrm{Ni}})$, which is a good approximation for an interface between crystals of different lattice parameters but identical elastic constants [24, 36, 46], is marked by a cross symbol.

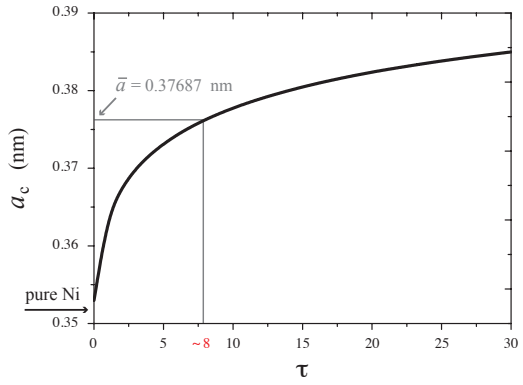


Figure 12: Dependence of the coherent lattice parameter of a Al−Ni heterophase interface as the stiffness constant $c_{11}$ of Al is artificially varied, such that $(\tau \times_{\mathrm{Al}} c_{11})$ (see text).

the non-arbitrary reference state, within which the Burgers vectors of individual interface dislocations are defined. A solution strategy is also formulated to predict the correct reference state in accordance with the duality {geometry−elasticity} in the description of anisotropic bicrystals. At equilibrium, the coherency strain fields are eliminated by the far-field strains produced by Volterra dislocations in the reference state, whereas the far-field rotations are consistent with a prescribed misorientation. In this viewpoint, the geometric structures of interfaces, including dislocation directions, spacing, characters and the magnitude of the Burgers vectors, are described in terms of elastic distortions in the case of heterogeneous anisotropic linear elasticity.

The complete elastic fields are found by using the Stroh formalism with Fourier series, where the long-range contributions (strains and rotations) are derived by calculated solutions in the far-field limits. The concept of partitioning of elastic distortions between adjacent crystals is also considered, especially for pure interfaces where the individual anisotropic moduli are different by nature. It implies than the elastic strains cannot be equally partitioned, as it has been usually assumed in many analyses. These considerations are used to compute elastic strain energies of infinite interface dislocation arrays, such as the pioneered works [21, 40, 54]. For a given interface where the number of solutions that satisfy the condition of removal of far-field strains is not unique, the determination of the minimum elastic energy of all possible configurations may be considered as a criteria in which case the interface with the lowest energy should be favored. These applications related to, for example, fcc−bcc interfaces, are to be presented in a follow-on study by comparing our results with atomistic simulations.

Some examples related to pure tilt and twist grain boundaries as well as pure misfit interfaces have been presented. Concerning the grain boundaries, it has been shown that our model is in good agreement with the "median lattice" suggested by Frank [22], for which the total rotations are partitioned equally between the two grains. The tilt boundary energy in Cu has been compared with experimental values and Read-Shockley solution. The results give rise to discuss about the important role played by our only core cutoff parameter when the rotation angle becomes large and the core energy becomes dominant. For twist grain boundaries, it has been shown that the introduction of a second set of screw dislocations to form an orthogonal grid of dislocations cancels the far-field strain fields. This non-surprising result validates our approach for interfaces containing two sets of dislocations. Results about FeNb?. The pure misfit interface study showed that the heterophase nature of interface has to be taken into account to find the correct reference state, because of the difference in the elastic constants of the two materials. A significant discrepancy may arise for moderately high and high anisotropic systems, when the calculations are performed by assuming the homogeneous elastic approximation of coherency and dislocation fields in the overall bicrystals.

In the future, we suggest incorporating in the present formalism more of the complexities. The following main perspectives can be drawn.

1. Further refinements are needed to establish the equilibrium forms of a simple fcc twist grain boundary about a $\langle 111 \rangle$ axis. Thus, the elastic relaxation by reactions of the intersecting dislocations should be taken into account. Comparisons with molecular dynamics simulations, sophisticated dislocation dynamics or phase field approaches could also be performed.
2. The couple stresses may be formulated in the present theory and the effects on the determination of the reference state and the calculation elastic strain energy of interface dislocations may be investigated.
3. Free surfaces and unequal layer thicknesses may be included to address the distribution of the elastic fields in multilayered crystals.
4. Elastic interaction between interface dislocation arrays and point defect in epitaxial systems may be determined to develop quantitative figures-of-merit for the defect sink strength of interfaces and to design (nano)structured materials with tailored response at irradiation.

5. The dislocation core energies may be described and characterized with respect to the elastic contributions by regularizing the core singularities.

## 7. Acknowledgements

We thank the following individual for fruitful discussions: R. Bonnet, W. Cai, J.P. Hirth, R.G. Hoagland, X.-Y. Liu, R.C. Pond, J. Wang, A. Rollett. This research was funded by the U.S. Department of Energy, Office of Science, Office of Basic Energy Sciences under Award No. 2008LANL1026 through the *Center for Materials at Irradiation and Mechanical Extremes*, an Energy Frontier Research Center at Los Alamos National Laboratory.

## Appendix A. Complete elastic field solutions

The complete solutions for elastic fields associated with a network consisting of two sets of dislocations is treated by applying the sextic formalism pioneered by Stroh [51]. It offers an elegant and powerful tool for finding elastic displacement fields that can then be used to obtain the distortion and stress fields in three dimensions. For non-zero wave vectors $\boldsymbol{k}$, the standard solutions satisfying eq. (9) can be written in the form [14]

$$\boldsymbol{u_k}(x_2) = \mathrm{e}^{i2\pi p x_2}\,\boldsymbol{a}\ , \tag{A-1}$$

where $p$ and $\boldsymbol{a}$ become the unknowns of the boundary value problem. Introducing eq. (A-1) into eq. (9), the vector $\boldsymbol{a}$ is found to satisfy the following homogeneous linear system

$$\underbrace{\left(\mathbf{W}_1 + p\left(\mathbf{W}_2 + \mathbf{W}_2^{\mathrm{t}}\right) + p^2\,\mathbf{W}_3\right)}_{\mathbf{\Pi}}\boldsymbol{a} = \mathbf{0}\ , \tag{A-2}$$

which is an eigenvalue problem with $p$ as the unknown [51, 53]. A non-trivial solution can be found only if

$$\det\mathbf{\Pi} = 0\ . \tag{A-3}$$

This leads to a sextic equation. Due to the positive definiteness of elastic strain energy, the solutions of eq. (A-3) have 6 imaginary roots, which occur in complex conjugates [18]. It is convenient to arrange the three first solutions $p^\alpha$ to have positive imaginary parts, indexed by superscripts $\alpha = 1, 2, 3$. The remaining three solutions have negative imaginary parts, so that $p^{\alpha+3} = p_*^\alpha$ where $_*$ indicates complex conjugation. The corresponding vectors $\boldsymbol{a}^\alpha$ are also complex conjugates with $\boldsymbol{a}^{\alpha+3} = \boldsymbol{a}_*^\alpha$, so that the general solution may be rewritten as a linear combination of the three eigenfunctions

$$\boldsymbol{u_k}(x_2) = \frac{1}{i2\pi}\sum_{\alpha=1}^{3}\lambda^\alpha \mathrm{e}^{i2\pi p^\alpha x_2}\,\boldsymbol{a}^\alpha + \zeta^\alpha \mathrm{e}^{i2\pi p_*^\alpha x_2}\,\boldsymbol{a}_*^\alpha\ . \tag{A-4}$$

Here, $\lambda^\alpha$ and $\zeta^\alpha$ are complex scaling parameters that depend on boundary conditions. Substituting eq. (A-4) into eq. (7), the complete elastic displacement field may be written in terms of a biperiodic Fourier series expansion, i.e.

$$\begin{aligned}\boldsymbol{u}_{\mathrm{tot}}(\boldsymbol{x}) = \boldsymbol{u}_0 + \mathbf{D}_{\mathrm{c}}\,\boldsymbol{x} + \frac{1}{i2\pi}\sum_{\boldsymbol{k}\neq\mathbf{0}}\mathrm{e}^{i2\pi\boldsymbol{k}\cdot\boldsymbol{r}} \\ \times\sum_{\alpha=1}^{3}\lambda^\alpha \mathrm{e}^{i2\pi p^\alpha x_2}\,\boldsymbol{a}^\alpha + \zeta^\alpha \mathrm{e}^{i2\pi p_*^\alpha x_2}\,\boldsymbol{a}_*^\alpha\ .\end{aligned} \tag{A-5}$$

The elastic distortion derived from eq. (A-5) is therefore

$$\begin{aligned}\mathbf{D}_{\mathrm{tot}}(\boldsymbol{x}) = \mathbf{D}_{\mathrm{c}} + \sum_{\boldsymbol{k}\neq\mathbf{0}}\mathrm{e}^{i2\pi\boldsymbol{k}\cdot\boldsymbol{r}} \\ \times\sum_{\alpha=1}^{3}\lambda^\alpha \mathrm{e}^{i2\pi p^\alpha x_2}\,\mathbf{G}^\alpha + \zeta^\alpha \mathrm{e}^{i2\pi p_*^\alpha x_2}\,\mathbf{G}_*^\alpha\ ,\end{aligned} \tag{A-6}$$

where the complex matrices $\mathbf{G}^\alpha = G_{kl}^\alpha$ are defined by

$$G_{kl}^\alpha = a_k^\alpha\left(k_1\,\delta_{l1} + k_3\,\delta_{l3} + p^\alpha\,\delta_{l2}\right)\ , \tag{A-7}$$

for the same wave vector $\boldsymbol{k}$. Moreover, the associated complete stress field is obtained by using Hooke's law

$$\begin{aligned}\boldsymbol{\sigma}_{\mathrm{tot}}(\boldsymbol{x}) &= \boldsymbol{\sigma}_{\mathrm{c}} + \sum_{\boldsymbol{k}\neq\mathbf{0}}\mathrm{e}^{i2\pi\boldsymbol{k}\cdot\boldsymbol{r}}\sum_{\alpha=1}^{3}\lambda^\alpha \mathrm{e}^{i2\pi p^\alpha x_2}\,\mathbf{H}^\alpha + \zeta^\alpha \mathrm{e}^{i2\pi p_*^\alpha x_2}\,\mathbf{H}_*^\alpha \\ &= \boldsymbol{\sigma}_{\mathrm{c}} + \boldsymbol{\sigma}^\sharp(\boldsymbol{x})\ ,\end{aligned} \tag{A-8}$$

where $\boldsymbol{\sigma}^\sharp$ is the short-range stress field and the coherency stress field $\boldsymbol{\sigma}_{\mathrm{c}}$ is related to the coherency strain, i.e. $\{\mathbf{D}_{\mathrm{c}}\} = \mathbf{E}_{\mathrm{c}}$, by

$$\boldsymbol{\sigma}_{\mathrm{c}} = \mathbb{C} : \{\mathbf{D}_{\mathrm{c}}\}\ , \tag{A-9}$$

and the matrices $\mathbf{H}^\alpha = H_{kl}^\alpha$ are defined by

$$H_{kl}^\alpha = \left(k_1\,c_{klj1} + k_3\,c_{klj3} + p^\alpha\,c_{klj2}\right)a_j^\alpha\ . \tag{A-10}$$

## Appendix B. Far-field solutions for interface dislocations

The far-field elastic fields for dislocation arrays are obtained from the complete expressions derived in Appendix A by determining separately the contribution of each set of dislocations when $x_2 \to \pm\infty$ and then superposing the individual solutions. The total displacement field for two sets of parallel dislocations may be rewritten as

$$\boldsymbol{u}_{\mathrm{dis}}(x_1,x_2,x_3) = \boldsymbol{u}_{\mathrm{dis}\,1}(x_1,x_2) + \boldsymbol{u}_{\mathrm{dis}\,2}(x_1,x_2,x_3)\ , \tag{B-1}$$

where subscripts $_{\mathrm{dis}\,1}$ and $_{\mathrm{dis}\,2}$ denote the individual sets of dislocations 1 and 2. Each individual displacement field may be determined by requiring $|\boldsymbol{p}_1^0| \to \infty$ or $|\boldsymbol{p}_2^0| \to \infty$ in eq. (6), giving

$$\begin{aligned}\boldsymbol{u}_{\mathrm{dis}\,1}(x_1,x_2) &= \sum_{n=-\infty}^{\infty}\mathrm{e}^{i2\pi k_n x_1}\,\boldsymbol{u}_n(x_2) \\ \boldsymbol{u}_{\mathrm{dis}\,2}(x_1,x_2,x_3) &= \sum_{m=-\infty}^{\infty}\mathrm{e}^{i2\pi(k_m x_1 + k_3 x_3)}\,\boldsymbol{u}_m(x_2)\ ,\end{aligned} \tag{B-2}$$

where $k_n$, $k_m$ and $k_3$ are the three wavelengths defined in eq. (6):

$$k_n = \frac{n \csc\phi}{|\boldsymbol{p}_1^0|} \ , \quad k_m = -\frac{m \operatorname{ctg}\phi}{|\boldsymbol{p}_2^0|} \quad \text{and,} \quad k_3 = \frac{m}{|\boldsymbol{p}_2^0|} \ . \tag{B-3}$$

Without loss of generality, we restrict the calculation to set 1. From Appendix A, the displacements $\boldsymbol{u}_n(x_2)$ in eq. (B-2a) are non-trivial solutions of the second-order differential eq. (9), written here as

$$\begin{aligned} \mathbf{0} = &-4\pi^2 k_n^2 \, \mathbf{C}_1 \, \boldsymbol{u}_n(x_2) + i2\pi k_n \left(\mathbf{C}_2 + \mathbf{C}_2^{\mathsf{t}}\right) \frac{\partial \boldsymbol{u}_n(x_2)}{\partial x_2} \\ &+ \mathbf{C}_3 \, \frac{\partial^2 \boldsymbol{u}_n(x_2)}{\partial x_2^2} \ , \end{aligned} \tag{B-4}$$

with $\mathbf{C}_1 = c_{j1k1}$, $\mathbf{C}_2 = c_{j1k2}$ and $\mathbf{C}_3 = c_{j2k2}$. Similar to expression (A-4), the most general solution of eq. (B-4) is the linear combination of eigenfunctions

$$\boldsymbol{u}_n(x_2) = \frac{1}{i2\pi n} \sum_{\alpha=1}^{3} \bar{\lambda}_1^\alpha \mathrm{e}^{i2\pi k_n p_1^\alpha x_2} \, \boldsymbol{a}_1^\alpha + \bar{\zeta}_1^\alpha \mathrm{e}^{i2\pi k_n p_{1*}^\alpha x_2} \, \boldsymbol{a}_{1*}^\alpha \ , \tag{B-5}$$

where the 6 complex eigenvalues $p_1^\alpha$ and the corresponding eigenvectors $\boldsymbol{a}_1^\alpha$ are determined by solving the two following equations:

$$\begin{matrix} \det \boldsymbol{\Pi}_1 = 0 \\ \boldsymbol{\Pi}_1 \boldsymbol{a}_1^\alpha = \mathbf{0} \end{matrix} \quad \text{with,} \quad \boldsymbol{\Pi}_1 = \mathbf{C}_1 + p_1 \left(\mathbf{C}_2 + \mathbf{C}_2^{\mathsf{t}}\right) + p_1^2 \, \mathbf{C}_3 \ . \tag{B-6}$$

Here, the subscript $_{\text{dis}}$ in eqs. (B-5−B-6) is omitted for clarity. Unlike $\lambda^\alpha$ and $\zeta^\alpha$ to eq. (A-4), the complex constants $\bar{\lambda}_1^\alpha$ and $\bar{\zeta}_1^\alpha$ in eq. (B-5) have been divided by $n \neq 0$ [11]. This operation is convenient when evaluating the sum over $n$ of eq. (B-2a). The elastic distortion field is then obtained by differentiation of eq. (B-2a) and (B-5):

$$\begin{aligned} \mathbf{D}_{\text{dis}\,1}(x_1, x_2) = d_1^{-1} \sum_{n=-\infty}^{\infty} &\mathrm{e}^{i2\pi k_n x_1} \sum_{\alpha=1}^{3} \bar{\lambda}_1^\alpha \mathrm{e}^{i2\pi k_n p_1^\alpha x_2} \, \mathbf{G}_1^\alpha \\ &+ \bar{\zeta}_1^\alpha \mathrm{e}^{i2\pi k_n p_{1*}^\alpha x_2} \, \mathbf{G}_{1*}^\alpha \ . \end{aligned} \tag{B-7}$$

Here, $d_1 = |\boldsymbol{p}_1^0| \cos\phi$ and $\mathbf{G}_1^\alpha = G_{1kl}^\alpha$ are $3 \times 3$ complex matrices defined by

$$G_{1kl}^\alpha = a_{1k}^\alpha \left(\delta_{l1} + p_1^\alpha \delta_{l2}\right) \ . \tag{B-8}$$

The sum over $n$ in eq. (B-7) may be calculated analytically, so the far-field distortion $\mathbf{D}_{\text{dis}\,1}^\infty$ is

$$\mathbf{D}_{\text{dis}\,1}^\infty = -\operatorname{sgn}(x_2) \ d_1^{-1} \sum_{\alpha=1}^{3} \bar{\lambda}_1^\alpha \mathbf{G}_1^\alpha + \bar{\zeta}_1^\alpha \mathbf{G}_{1*}^\alpha \ . \tag{B-9}$$

Similar results are found for the elastic distortion produced by set 2. The total far-field distortion is obtained by adding the contributions of both dislocation sets:

$$\begin{aligned} \mathbf{D}_{\text{dis}}^\infty &= \mathbf{D}_{\text{dis}\,1}^\infty + \mathbf{D}_{\text{dis}\,2}^\infty \\ &= -\operatorname{sgn}(x_2) \ \mathrm{Re} \sum_{i=1}^{2} d_i^{-1} \sum_{\alpha=1}^{3} \bar{\lambda}_i^\alpha \mathbf{G}_i^\alpha + \bar{\zeta}_i^\alpha \mathbf{G}_{i*}^\alpha \ , \end{aligned} \tag{B-10}$$

where the matrices $\mathbf{G}_2^\alpha = G_{2kl}^\alpha$ are defined by

$$G_{2kl}^\alpha = a_{2k}^\alpha \left(-\cos\phi \ \delta_{l1} + \sin\phi \ \delta_{l3} + p_2^\alpha \delta_{l2}\right) \ . \tag{B-11}$$

The complex eigenvalues $p_2^\alpha$ and eigenvectors $\boldsymbol{a}_2^\alpha$ are determined by solving eqs. (B-6) with the associated matrix $\boldsymbol{\Pi}_2$ defined by

$$\boldsymbol{\Pi}_2 = \mathbf{C}_{1(2)} + p_1 \mathbf{C}_{2(2)} + p_1^2 \mathbf{C}_{3(2)} \ , \tag{B-12}$$

where

$$\begin{aligned} \mathbf{C}_{1(2)} &= \cos^2\phi \ c_{j1k1} + \sin^2\phi \ c_{j3k3} - \tfrac{1}{2} \sin 2\phi \ \{c_{j1k3}\} \\ \mathbf{C}_{2(2)} &= -\cos\phi \ \{c_{j1k2}\} + \sin\phi \ \{c_{j2k3}\} \\ \mathbf{C}_{3(2)} &= \mathbf{C}_3 = c_{j2k2} \ . \end{aligned} \tag{B-13}$$

According to eq. (B-10), the overall long-range stress field produced by set $1+2$ in both half-spaces is

$$\begin{aligned} \boldsymbol{\sigma}_{\text{dis}}^\infty &= \boldsymbol{\sigma}_{\text{dis}\,1}^\infty + \boldsymbol{\sigma}_{\text{dis}\,2}^\infty \\ &= -\operatorname{sgn}(x_2) \sum_{i=1}^{2} d_i^{-1} \ \mathrm{Re} \sum_{\alpha=1}^{3} \bar{\lambda}_i^\alpha \mathbf{H}_i^\alpha + \bar{\zeta}_i^\alpha \mathbf{H}_{i*}^\alpha \ , \end{aligned} \tag{B-14}$$

where $\mathbf{H}_1^\alpha = H_{1kl}^\alpha$ and $\mathbf{H}_2^\alpha = H_{2kl}^\alpha$ are defined by

$$\begin{aligned} H_{1kl}^\alpha &= \left(c_{klj1} + p_1^\alpha \, c_{klj2}\right) a_{1k}^\alpha \\ H_{2kl}^\alpha &= \left(-\cos\phi \ c_{klj1} + \sin\phi \ c_{klj3} + p_2^\alpha \, c_{klj2}\right) a_{2k}^\alpha \ . \end{aligned} \tag{B-15}$$

Finally, to obtain the complete far-field solutions of the distortions by eq. (B-10) and the stresses by eq. (B-14), the 24 remaining unknown complex constants, i.e.

$$\bar{\mathrm{E}}\mathrm{cst} = \left\{ \mathrm{Re}\,{}_{\mathrm{A}}\bar{\lambda}_i^\alpha, \mathrm{Im}\,{}_{\mathrm{A}}\bar{\lambda}_i^\alpha, \mathrm{Re}\,{}_{\mathrm{B}}\bar{\zeta}_i^\alpha, \mathrm{Im}\,{}_{\mathrm{B}}\bar{\zeta}_i^\alpha \right\} \ , \tag{B-16}$$

for $\alpha \in \{1,2,3\}$ and $i \in \{1,2\}$, are found by solving the two following linear systems of 12 equations for each wave vector $\boldsymbol{k} \neq \mathbf{0}$:

$$\Sigma_{1+2}^\infty : \begin{cases} \mathrm{Re} \sum_{\boldsymbol{k}\neq\mathbf{0}} \sum_{\alpha=1}^{3} {}_{\mathrm{A}}\bar{\lambda}_i^\alpha \, {}_{\mathrm{A}}\boldsymbol{a}_i^\alpha - {}_{\mathrm{B}}\bar{\zeta}_i^\alpha \, {}_{\mathrm{B}}\boldsymbol{a}_{i*}^\alpha = -\boldsymbol{b}_i \\ \mathrm{Im} \sum_{\boldsymbol{k}\neq\mathbf{0}} \sum_{\alpha=1}^{3} {}_{\mathrm{A}}\bar{\lambda}_i^\alpha \, {}_{\mathrm{A}}\boldsymbol{a}_i^\alpha - {}_{\mathrm{B}}\bar{\zeta}_i^\alpha \, {}_{\mathrm{B}}\boldsymbol{a}_{i*}^\alpha = \mathbf{0} \\ \mathrm{Re} \sum_{\boldsymbol{k}\neq\mathbf{0}} \sum_{\alpha=1}^{3} {}_{\mathrm{A}}\bar{\lambda}_i^\alpha \, {}_{\mathrm{A}}\boldsymbol{h}_i^\alpha - {}_{\mathrm{B}}\bar{\zeta}_i^\alpha \, {}_{\mathrm{B}}\boldsymbol{h}_{i*}^\alpha = \mathbf{0} \\ \mathrm{Im} \sum_{\boldsymbol{k}\neq\mathbf{0}} \sum_{\alpha=1}^{3} {}_{\mathrm{A}}\bar{\lambda}_i^\alpha \, {}_{\mathrm{A}}\boldsymbol{h}_i^\alpha - {}_{\mathrm{B}}\bar{\zeta}_i^\alpha \, {}_{\mathrm{B}}\boldsymbol{h}_{i*}^\alpha = \mathbf{0} \ , \end{cases} \tag{B-17}$$

according to the *conditions 3.* and *4.* for specific requirements at the interface, as discussed in section 4.4. The vectors $\boldsymbol{h}^\alpha$ are related to $\mathbf{H}^\alpha$ by

$$h_{1k}^\alpha = H_{1k2}^\alpha \quad \text{and,} \quad h_{2k}^\alpha = H_{2k2}^\alpha \ . \tag{B-18}$$

## References


[1] Amelinckx S. The direct observation of dislocations. New-York: Academic Press; 1964.
[2] Argon AS. Strengthening mechanisms in crystal plasticity. Oxford ; New-York: Oxford University Press; 2008.
[3] Barnett DM, Lothe J, Phys Norv 1975; 8:13.
[4] Bilby BA, Bullough R, Smith E. Proc Roy Soc A (London) 1955; 231:263.
[5] Brillson LJ. Surf Sci Rep 1982; 2:123.
[6] Bollmann W. Crystal defects and crystalline interfaces. Berlin: Springer-Verlag; 1970.
[7] Bollmann W. Phys Stat Sol A 1974; 21:543.
[8] Bonnet R, Dupeux M. Philos Mag 1980; 42:809.
[9] Bonnet R. Acta Metall 1981; 29:437.
[10] Bonnet R. Philos Mag A 1981; 43:1165.
[11] Bonnet R. Philos Mag A 1985; 51:51.
[12] Burgers WG. Physica 1 1934; 561.
[13] Chou YT. J Appl Phys 1962; 33:2747.
[14] Churchill RV. Fourier Series and Boundary Value Problems. New-York: McGraw-Hill; 1963.
[15] Comninou M, Dundurs J. J Appl Mech 1977; 44:222.
[16] Demkowicz MJ, Wang J, Hoagland RG. Interfaces between dissimilar crystalline solids. Dislocations in Solids, edited by Hirth JP. Amsterdam: Elsevier, vol. 14, p. 141; 2008.
[17] Demkowicz MJ, Thilly L. Acta Mater 2011; 59:7744.
[18] Eshelby JD, Read WT, Shockley W, Acta Metall 1953; 1:251.
[19] Fletcher NH. Crystal interface models − a critical survey. Advances in Materials Research, edited by H. Herman. New-York: Wiley-Interscience Publisher, p. 281; 1971.
[20] Fors DHR, Johansson SAE, Petisme MVG, Wahnström G. Comput Mat Sci 2010 ;50:550.
[21] Frank FC, van der Merwe JH. Proc Roy Soc A (London) 1949; 198:205.
[22] Frank FC. The resultant content of dislocations in an arbitrary intercrystalline boundary. A symposium on the plastic deformation of crystalline solids. Office of Naval Research, Pittsburgh, PA, p. 150; 1950.
[23] Frank FC. Philos Mag 1951; 42:809.
[24] Frank FC. Acta Metall 1953; 1:15.
[25] Gjostein NA, Rhines FN. Acta Metall 1959; 7:319.
[26] Gray DE, American Institute of Physics Handbook. New-York: MacGraw-Hill; 1957.
[27] Hall MG, Rigsbee JM, Aaronson HI. Acta Metall 1986; 34:1419.
[28] Hirth JP, Balluffi RW. Acta Metall 1973; 21:929.
[29] Hirth JP, Barnett DM, Lothe J. Philos Mag A 1979; 40:39.
[30] Hirth JP, Lothe J. Theory of Dislocations. 2nd ed. Melbourne: Kriger; 1992.
[31] Hirth JP, Pond RC. Philos Mag Let 2010; 23:3129;
[32] Hirth JP, Pond RC. Prog Mater Sci 2011; 56:586.
[33] Hirth JP, Pond RC, Hoagland RG, Liu XY, Wang J. Prog Mater Sci 2013; 58:749.
[34] Hoagland RG, Kurtz RJ. Philos Mag A 2002; 82:1073.
[35] Inderjeet K, Mishin Y, Gust W. Fundamentals of Grain and Interphase Boundary Diffusion. New-York: Wiley; 1995.
[36] Jesser WA. Phys Stat Sol 1973; 20:63.
[37] Knowles KM. Philos Mag A 1982; 46:951.
[38] Kolluri K, Demkowicz M. Phys Rev B 2010; 82:193404.
[39] Li JCM. Acta Metall 1960; 8:563.
[40] Lubarda VA, Int J Solids Struct 1997; 34:1053.
[41] Masumura RA, Glicksman ME. J Electron Mater 1975; 4:823.
[42] Matthews JW, Blakeslee AE. J Cryst Growth 1974; 27:118.
[43] Matthews JW, Blakeslee AE. J Cryst Growth 1975; 29:273.
[44] Matthews JW, Blakeslee AE. J Cryst Growth 1976; 32:265.
[45] Matthews JW, Blakeslee AE, Mader S. Thin Solid Films 1976; 33:253.
[46] Matthews JW. Acta Metall, 1976; 24:381.
[47] Olson GB, Cohen M. Acta Metall 1979; 27:1907.
[48] Read WT, Shockley W. Phys Rev 1950; 78:275.
[49] Read WT, Shockley W. Imperfections in nearly perfect crystals. New-York: Wiley; 1952.
[50] Siegel RW, Chang SM, Balluffi RW. Acta Metall 1980; 28:249.
[51] Stroh AN. Philos Mag 1958; 3:625.
[52] Sutton AP, Balluffi RW. Interfaces in Crystalline Materials. Oxford: Oxford University Press; 1995.
[53] Ting TCT. Anisotropic Elasticity. Oxford University Press, New-York, 1996.
[54] van der Merwe JH. Proc Roy Soc A (London) 1950; 63:616.
[55] Winchell PG, Boah J, Ayres PS. J Appl Phys 1970; 42:2612.
[56] Yang JB, Nagai Y, Yang ZG, Hasegawa M. Acta Mater 2009; 57:4874.
[57] Zhang WZ, Purdy. Acta Metall Mater 1993; 41:543;